Nucleon Axial Radius and Muonic Hydrogen

Richard J. Hill[1,2,3], Peter Kammel[4], William J. Marciano[5], and Alberto Sirlin[6]

[1]*Department of Physics and Astronomy, University of Kentucky, Lexington, KY 40506, USA*
[2]*Fermilab, Batavia, IL 60510, USA*
[3]*Perimeter Institute for Theoretical Physics, Waterloo, ON N2L 2Y5 Canada*
[4]*Center for Experimental Nuclear Physics and Astrophysics and Department of Physics, University of Washington, Seattle, WA 98195, USA*
[5]*Department of Physics, Brookhaven National Laboratory, Upton, NY 11973, USA*
[6]*Department of Physics, New York University, New York, NY 10003 USA*

August 28, 2017

Abstract

Weak capture in muonic hydrogen (μH) as a probe of the chiral properties and nucleon structure predictions of Quantum Chromodynamics (QCD) is reviewed. A recent determination of the axial-vector charge radius squared, $r_A^2(z\ \text{exp.}) = 0.46(22)\ \text{fm}^2$, from a model independent z expansion analysis of neutrino-nucleon scattering data is employed in conjunction with the MuCap measurement of the singlet muonic hydrogen capture rate, $\Lambda_{\text{singlet}}^{\text{MuCap}} = 715.6(7.4)\ \text{s}^{-1}$, to update the induced pseudoscalar nucleon coupling: $\bar{g}_P^{\text{MuCap}} = 8.19(84)$ derived from experiment, and $\bar{g}_P^{\text{theory}} = 8.25(25)$ predicted by chiral perturbation theory. Accounting for correlated errors this implies $\bar{g}_P^{\text{theory}}/\bar{g}_P^{\text{MuCap}} = 1.01(8)$, confirming theory at the 8% level. If instead, the predicted expression for $\bar{g}_P^{\text{theory}}$ is employed as input, then the capture rate alone determines $r_A^2(\mu\text{H}) = 0.43(24)\,\text{fm}^2$, or together with the independent z expansion neutrino scattering results, a weighted average $r_A^2(\text{ave.}) = 0.45(16)\,\text{fm}^2$. Sources of theoretical uncertainty are critically examined and potential experimental improvements are described that can reduce the capture rate error by about a factor of 3. Muonic hydrogen can thus provide a precise and independent r_A^2 value which may be compared with other determinations, such as ongoing lattice gauge theory calculations. The importance of an improved r_A^2 determination for phenomenology is illustrated by considering the impact on critical neutrino-nucleus cross sections at neutrino oscillation experiments.

Contents

1 Introduction

Muonic hydrogen, the electromagnetic bound state of a muon and proton, is a theoretically pristine atomic system. As far as we know, it is governed by the same interactions as ordinary hydrogen, but with the electron of mass 0.511 MeV replaced by the heavier muon of mass 106 MeV, an example of electron-muon universality. That mass enhancement ($\sim$207) manifests itself in much larger atomic energy spacings and a smaller Bohr radius of 2.56×10^{-3}Å. This places the muonic hydrogen size about halfway (logarithmically) between the atomic angstrom and the nuclear fermi (1 fm = 10^{-5}Å) scale.

Those differences make muonic hydrogen very sensitive to otherwise tiny effects such as those due to proton size and nucleon structure parameters governing weak interaction phenomenology. Indeed, muonic hydrogen Lamb shift spectroscopy [1, 2] has provided a spectacularly improved measurement of the proton charge radius that differs by about 7 standard deviations from the previously accepted value inferred from ordinary hydrogen and electron-proton scattering [3]. (That so called Proton Radius Puzzle is currently unresolved [4–6]). Similarly, the larger muon mass kinematically allows the weak muon capture process depicted in Fig. 1,

$$\mu^- + p \to \nu_\mu + n\,, \tag{1}$$

to proceed, while ordinary hydrogen is (fortunately for our existence) stable.

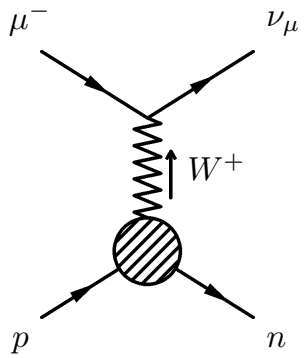

Figure 1: Muon capture on the proton, $\mu^- p \to \nu_\mu n$, via charged W boson exchange.

Weak muon capture in nuclei has provided a historically important probe of weak interactions and a window for studying nuclear structure. In particular, weak capture in muonic hydrogen is a sensitive probe of the induced pseudoscalar component of the axial current $p \to n$ matrix element which is well predicted from the chiral properties of QCD. However, early experimental determinations of that pseudoscalar coupling, $\bar{g}_P$,[1] had, for some time, appeared problematic [7]. All $\bar{g}_P$ extractions from ordinary muon capture in hydrogen suffered from limited precision, while the more sensitive extraction from radiative muon capture [8] disagreed with ordinary muon capture and the solid prediction of Chiral Perturbation Theory (χPT) [9–13]. An important underlying contribution to this problem was the chemical activity of muonic hydrogen, which like its electronic sibling, can form molecular ions, $(pp\mu)^+$. The highly spin dependent weak interaction leads to very different capture rates from various muonic atomic and molecular states. Thus, atomic physics processes like ortho-para transitions in the muonic molecule, which flip the proton spins, significantly change the observed weak capture rates and often clouded the interpretation of experimental results in the 55-year history of this field. Unfortunately, the uncertainty induced by molecular transitions was particularly severe for the most precise measurements which were performed with high density liquid hydrogen targets, where, because of rapid $pp\mu$ formation, essentially capture from the molecule, not the $p\mu$ atom, is observed. This problem was resolved by the MuCap Collaboration at

[1]The quantity $\bar{g}_P$ is defined at the characteristic momentum q_0^2 for muon capture, see Eqs. (8),(23) below.

the Paul Scherrer Institute (PSI) which introduced an active, in situ, target, where ultra-pure hydrogen gas served both as the target as well as the muon detector, thus enabling a measurement of the muonic hydrogen capture rate at low density, where $pp\mu$ formation is suppressed. MuCap unambiguously determined the spin singlet muonic hydrogen capture rate $\Lambda_{\rm singlet}^{\rm MuCap} = 715.6(7.4)\,{\rm s}^{-1}$ [14, 15] to 1% accuracy which, when corrected for an enhancement from radiative corrections [16], and using prevailing form factor values at the time implied $\bar{g}_P^{\rm MuCap} = 8.06(55)$, in excellent agreement with $\bar{g}_P^{\rm theory} = 8.26(23)$, the predicted value.

We note, however, that the determination of $\bar{g}_P$ from both experiment and theory required the input of the axial charge radius squared, traditionally taken from dipole form factor fits to neutrino-nucleon quasielastic charged current scattering ($\nu_\mu n \to \mu p$) and pion electroproduction ($eN \to eN'\pi$) data, which at the time implied the very precise [17] $r_A^2({\rm dipole}) = 0.454(13)\,{\rm fm}^2$. Recently, that small ($\sim 3\%$) uncertainty in r_A^2 has been called into question, since it derives from the highly model dependent dipole form factor assumption.[2] The axial radius, which is central to this paper, governs the momentum dependence of the axial-vector form factor, by means of the expansion at small q^2,

$$F_A(q^2) = F_A(0)\left(1 + \frac{1}{6} r_A^2 q^2 + \dots\right) . \tag{2}$$

In the one-parameter dipole model, the terms denoted by the ellipsis in Eq. (2) are completely specified in terms of r_A^2. However, the true functional form of $F_A(q^2)$ is unknown, and the dipole constraint represents an uncontrolled systematic error. We may instead employ the z expansion formalism, a convenient method for enforcing the known complex-analytic structure of the form factor inherited from QCD, while avoiding poorly controlled model assumptions. This method replaces the dipole $F_A(q^2)$ with $F_A[z(q^2)]$, which in terms of the conformal mapping variable $z(q^2)$, has a convergent Taylor expansion for all spacelike q^2. The size of the expansion parameter, and the truncation order of the expansion necessary to describe data of a given precision in a specified kinematic range, are determined a priori. This representation helps ensure that observables extracted from data are not influenced by implicit form factor shape assumptions. Using the z expansion [18] to fit the neutrino data alone leads to [19] $r_A^2(z\ {\rm exp.},\ \nu) = 0.46(22)\,{\rm fm}^2$ with a larger ($\sim 50\%$), more conservative but better justified error. As we will discuss below, traditional analyses of pion electroproduction data have also used a dipole assumption to extract r_A^2 from $F_A(q^2)$, and in addition required the a priori step of phenomenological modeling to extract $F_A(q^2)$ from data. Since these model uncertainties have not been quantified, we refrain from including pion electroproduction determinations of r_A^2 in our analysis. Similarly, we do not include extractions from neutrino-nucleus scattering on nuclei larger than the deuteron, in order to avoid poorly quantified nuclear model uncertainties. In this context, we note that dipole fits to recent ν-C scattering data suggest a smaller $r_A^2 \approx 0.26\,{\rm fm}^2$ [20], compared to historical dipole values $r_A^2 \sim 0.45\,{\rm fm}^2$ [17]. This discrepancy may be due to form factor shape biases (i.e., the dipole assumption), mismodeling of nuclear effects, or something more interesting. Independent determination of r_A^2 is a necessary ingredient for resolving this discrepancy. Finally, we do not include recent interesting lattice QCD results [21–24], some of which suggest considerably smaller r_A^2 values. As we shall discuss below in Sec. 5, future improvements on these lattice QCD results could provide an independent r_A^2 value with controlled systematics, that would open new opportunities for interpreting muon capture. To illustrate the broad range of possible r_A^2 values, we provide in Table 1 some representative values considered in the recent literature.

Accepting the larger r_A^2 uncertainty from the z expansion fit to neutrino data, leads to renewed thinking about the utility of precision measurements of muonic hydrogen capture rates for probing QCD chiral properties. As we shall see, the determination of $\bar{g}_P$ becomes $\bar{g}_P^{\rm MuCap} = 8.19(84)$ and $\bar{g}_P^{\rm theory} = 8.25(25)$, which are still in good agreement, but with errors enlarged by factors of 1.7 and 3.5, respectively, compared to results using $r_A^2({\rm dipole})$ [cf. Eqs. (31),(32) below]. However, taking into account the correlated uncertainties, the comparison can be sharpened to $\bar{g}_P^{\rm theory}/\bar{g}_P^{\rm MuCap} = 1.01(8)$.

[2] The dipole ansatz corresponds to $F_A(q^2) = F_A(0)/(1 - q^2/m_A^2)^2$ with fit mass parameter m_A.

Table 1: Illustrative values obtained for r_A^2 from neutrino-deuteron quasi elastic scattering (ν-d), pion electroproduction ($eN \to eN'\pi$), neutrino-carbon quasielastic scattering (ν-C), muon capture (MuCap) and lattice QCD. Values labeled "dipole" enforce the dipole shape ansatz. The value labeled "z exp." uses the model independent z expansion.

Description	r_A^2 (fm^2)	Source/Reference
νd (dipole)	0.453(23)	[17]
$eN \to eN'\pi$ (dipole)	0.454(14)	[17]
average	0.454(13)	
νC (dipole)	0.26(7)	[20]
νd (z exp.)	0.46(22)	[19]
MuCap	0.43(24)	this work
average	0.45(16)	
lattice QCD	0.213(6)(13)(3)(0)	[21]
	0.266(17)(7)	[22]
	$0.360(36)^{+80}_{-88}$	[23]
	0.24(6)	[24]

Instead of determining $\bar{g}_P$, one can use the functional dependence of this quantity, $\bar{g}_P(r_A^2)$, predicted from χPT to extract r_A^2 from the singlet capture rate. As we shall show, that prescription currently gives a sensitivity to r_A^2 comparable to z-expansion fits to neutrino-nucleon scattering. We use the resulting value from muon capture to derive a combined weighted average. We also examine how such a method can be further improved by better theory and experiment, and demonstrate that a factor of $\sim$3 improvement in the experimental precision appears feasible and commensurate with our updated theoretical precision.

The axial radius is indispensable for ab-initio calculations of nucleon-level charged current quasielastic cross sections needed for the interpretation of long baseline neutrino oscillation experiments at $|q^2| \sim 1\,\mathrm{GeV}^2$. Its current uncertainty is a serious impediment to the extraction of neutrino properties from such measurements. We quantify the impact that an improved muon capture determination of r_A^2 would have on neutrino-nucleon cross sections, and discuss the status and potential for other determinations, particularly from the promising lattice QCD approach.

The remainder of this paper is organized as follows: In Sec. 2 we give an overview and update regarding the theory of μ-p capture in muonic hydrogen. We first discuss the lowest order formalism. We then outline the status of radiative corrections and argue for a reduction in the overall theory error on the capture rate to about $\pm 0.15\%$ based on new considerations. Uncertainties in the input parameters are described, with particular emphasis on a numerical analysis of the axial charge radius squared and its potential extraction from the singlet 1S capture rate in μH. Then, in Sec. 3, we describe the experimental situation. After reviewing the MuCap result, we discuss possible improvements for a next generation experiment that would aim for a further factor of $\sim$3 error reduction. In Sec. 4, we discuss what can be learned from the present MuCap result and an improved experiment. We update the determination of $\bar{g}_P$ from the MuCap measurement using the more conservative z expansion value of r_A^2 obtained from neutrino-nucleon scattering. Then, as a change in strategy, using the theoretical expression for $\bar{g}_P$ obtained from χPT as input, r_A^2 is extracted from the MuCap capture rate and averaged with the z expansion value. Other utilizations of MuCap results are also discussed. In Sec. 5, we illustrate the impact of an improved r_A^2 determination on quasielastic neutrino scattering cross sections and discuss the status of, and prospects

for, improving alternative r_A^2 determinations. Section 6 concludes with a summary of our results and an outlook for the future.

2 Muon capture theory update

The weak capture process, Eq. (1), from a muonic hydrogen bound state is a multi-scale field theory calculational problem, involving electroweak, hadronic and atomic mass scales. In this section, we review the essential ingredients of this problem before discussing the status of phenomenological inputs and the numerical evaluation of the capture rate.

2.1 Preliminaries

For processes at low energy, $E \ll m_W$, where $m_W \approx 80\,\mathrm{GeV}$ is the weak charged vector boson mass, the influence of heavy particles and other physics at the weak scale is rigorously encoded in the parameters of an effective Lagrangian containing four-fermion operators. For muon capture the relevant effective Lagrangian is

$$\mathcal{L} = -\frac{G_F V_{ud}}{\sqrt{2}} \bar{\nu}_\mu \gamma^\mu (1-\gamma_5) \mu \; \bar{d} \gamma_\mu (1-\gamma_5) u + \text{H.c.} + \dots \,, \tag{3}$$

where G_F and V_{ud} are the Fermi constant and the CKM up-down quark mixing parameter respectively (cf. Table 2), and the ellipsis denotes effects of radiative corrections. Atomic physics of the muonic hydrogen system is described by the effective Hamiltonian,

$$H = \frac{p^2}{2m_r} - \frac{\alpha}{r} + \delta V_{\mathrm{VP}} - i \frac{G_F^2 |V_{ud}|^2}{2} \left[c_0 + c_1 (\boldsymbol{s}_\mu + \boldsymbol{s}_p)^2 \right] \delta^3(\boldsymbol{r}) \,, \tag{4}$$

where $m_r = m_\mu m_p/(m_\mu + m_p)$ is the reduced mass, δV_{VP} accounts for electron vacuum polarization as discussed below, and $\boldsymbol{s}_\mu$, $\boldsymbol{s}_p$ are muon and proton spins. The annihilation process is described by an anti-Hermitian component of H [25]. Since the weak annihilation is a short-distance process compared to atomic length scales, this anti-Hermitian component can be expanded as a series of local operators. At the current level of precision terms beyond the leading one, $\delta^3(\boldsymbol{r})$, are irrelevant [25]. Relativistic corrections to the Coulomb interaction in Eq. (4) are similarly irrelevant [26]. In both cases, neglected operators contribute at relative order $v^2/c^2 \sim \alpha^2$, where v is the nonrelativistic bound state velocity. Electron vacuum polarization enters formally at order α^2, but is enhanced by a factor m_μ/m_e making it effectively a first order correction [27, 28].

Having determined the structure of the effective Hamiltonian (4), the numbers c_i are determined by a matching condition with the quark level theory (3). The annihilation rate in the 1S state is then computed from H to be

$$\Lambda = G_F^2 |V_{ud}|^2 \times [c_0 + c_1 F(F+1)] \times |\psi_{1\mathrm{S}}(0)|^2 + \dots \,, \tag{5}$$

where $|\psi_{1\mathrm{S}}(0)|^2 = m_r^3 \alpha^3/\pi$ is the ground state wavefunction at the origin squared and F is the total spin ($F = 0$ for singlet, $F = 1$ for triplet). Equation (5), with c_i expressed in terms of hadronic form factors (cf. Eq. (7) below), exhibits the factorization of the process into effects arising from weak, hadronic and atomic scales.

2.2 Tree level calculation

Hadronic physics in the nucleon matrix elements of the vector and axial-vector quark currents of Eq. (3) is parameterized as:[3]

$$\langle n|(V^\mu - A^\mu)|p\rangle = \bar{u}_n\Big[F_1(q^2)\gamma^\mu + \frac{iF_2(q^2)}{2m_N}\sigma^{\mu\nu}q_\nu - F_A(q^2)\gamma^\mu\gamma^5 - \frac{F_P(q^2)}{m_N}q^\mu\gamma^5 + \frac{F_S(q^2)}{m_N}q^\mu - \frac{iF_T(q^2)}{2m_N}\sigma^{\mu\nu}q_\nu\gamma^5\Big]u_p + \dots\,, \tag{6}$$

where $V^\mu - A^\mu = \bar{d}\gamma^\mu u - \bar{d}\gamma^\mu\gamma_5 u$, and the ellipsis again denotes effects of radiative corrections. For definiteness we employ the average nucleon mass $m_N \equiv (m_n + m_p)/2$. The form factors F_S and F_T are so-called second class amplitudes that violate G parity and are suppressed by isospin violating quark masses or electromagnetic couplings [30–33]. They would appear in the capture rate, Eq. (7) below, accompanied by an additional factor m_μ/m_N relative to F_1 and F_A. Similar to isospin violating effects in $F_2(0)$, discussed below in Sec. 2.4, power counting predicts negligible impact of F_S and F_T at the permille level; we thus ignore them in the following discussion.

The c_i in Eq. (5) are determined by matching the quark level theory (3) to the nucleon level theory (4), using the hadronic matrix elements (6). This matching is accomplished by enforcing, e.g., equality of the annihilation rate for $\mu p \to \nu_\mu n$ computed in both theories for the limit of free particles, with the proton and muon at rest. For the coefficients corresponding to singlet and triplet decay rates, this yields [16, 34]

$$\begin{aligned} c_0 &= \frac{E_\nu^2}{2\pi M^2}(M-m_n)^2\bigg[\frac{2M-m_n}{M-m_n}F_1(q_0^2) + \frac{2M+m_n}{M-m_n}F_A(q_0^2) - \frac{m_\mu}{2m_N}F_P(q_0^2) \\ &\quad + (2M+2m_n-3m_\mu)\frac{F_2(q_0^2)}{4m_N}\bigg]^2\,, \\ c_0+2c_1 &= \frac{E_\nu^2}{24\pi M^2}(M-m_n)^2\bigg\{\bigg[\frac{m_\mu}{m_N}F_P(q_0^2) - \frac{2m_n}{M-m_n}\big(F_1(q_0^2)-F_A(q_0^2)\big) \\ &\quad + (2M+2m_n-m_\mu)\frac{F_2(q_0^2)}{2m_N}\bigg]^2 + 2\bigg[\frac{m_\mu}{m_N}F_P(q_0^2) + \frac{2M}{M-m_n}\big(F_1(q_0^2)-F_A(q_0^2)\big) - m_\mu\frac{F_2(q_0^2)}{2m_N}\bigg]^2\bigg\}\,, \end{aligned} \tag{7}$$

where the initial state mass is $M \equiv m_\mu + m_p$, the neutrino energy is $E_\nu \equiv (M^2 - m_n^2)/2M = 99.1482$ MeV, and the invariant momentum transfer is

$$q_0^2 \equiv m_\mu^2 - 2m_\mu E_\nu = -0.8768\, m_\mu^2. \tag{8}$$

Since the matching is performed with free particle states, the quantities M, E_ν and q_0^2 are defined independent of the atomic binding energy, as necessary for determination of the state-independent coefficients c_i of the effective Hamiltonian (4).[4]

The amplitudes (7) can also be expressed as an expansion in χPT [12, 35–37]. However, the general formulas in Eq. (7) allow us to more directly implement and interpret experimental constraints on the form factors and do not carry the intrinsic truncation error of NNLO χPT derivations (estimated in Ref. [37] as $\pm 1\%$). For example, we may take the vector form factors F_1, F_2 directly from experimental data, rather than attempting to compute them as part of an expansion in χPT. No approximation is yet made in Eq. (7), except for neglect of second class currents, as justified above. We investigate below the restricted application of χPT to express $F_P(q_0^2)$ in terms of r_A^2 and other experimentally measured quantities.

[3] We choose a convention for the pseudoscalar form factor that is independent of lepton mass: $F_P(q^2) = (m_N/m_\mu)g_P(q^2)$, in terms of $g_P(q^2)$ used in Ref. [29]. Our sign conventions for F_A and F_P are such that $F_A(0)$ and all other form factors are positive.

[4] In particular, a binding energy is not included in the initial-state mass M, but would anyways correspond to a relative order α^2 correction that is beyond the current level of precision.

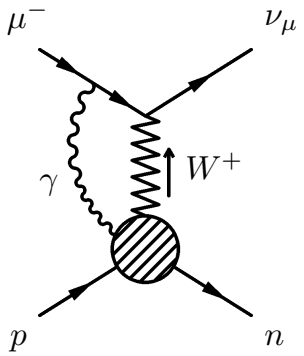

Figure 2: Example of an $\mathcal{O}(\alpha)$ γW exchange box diagram radiative correction to muon capture.

2.3 Radiative corrections

The electroweak radiative corrections to muon capture in muonic hydrogen, depicted in Fig. 2, were first calculated in Ref. [16]. Here, we briefly describe the origin of such quantum loop effects and take this opportunity to update and reduce their estimated uncertainty. The computational strategy relies on the well known electroweak corrections to (i) the muon lifetime [38, 39], (ii) super-allowed $0^+ \to 0^+$ β decays [38, 40, 41], and (iii) the neutron lifetime [42, 43].

Radiative corrections to weak decay processes in the Standard Model involve ultraviolet divergences that can be renormalized, yielding finite phenomenological parameters such as the Fermi constant G_F obtained from the measured muon lifetime [39] and the CKM matrix element $|V_{ud}|$ obtained from super-allowed β decays (see Table 2). In terms of those parameters, the radiative corrections to the neutron lifetime and the muon capture rate are rendered finite and calculable. We note that the matrix element of the vector current is absolutely normalized at $q^\mu = 0$, corresponding to a Conserved Vector Current (CVC): $F_1(0) = 1$, up to second order corrections in small isospin violating parameters [44–46]. On the other hand, the normalization of the remaining form factors appearing in Eq. (7) requires a conventional definition in the presence of radiative corrections. This definition is specified at $q^2 = 0$ by a factorization requirement that expresses the total process as a tree level expression times an overall radiative correction. For example, the neutron decay rate in this scheme involves the factor $(1+3g_A^2)(1+\mathrm{RC})$, where $(1+3g_A^2)$ is the tree level expression with $F_A(0) = g_A$, and RC denotes the radiative corrections. By the definition of g_A, these corrections are the same for vector and axial-vector amplitudes, but are actually computed for the vector amplitude. In that way, g_A can be obtained from the neutron lifetime, used in conjunction with V_{ud} via the relationship [41, 42]

$$\left(1 + 3g_A^2\right) |V_{ud}|^2 \tau_n = 4908.7(1.9)\ \mathrm{s}\,. \tag{9}$$

Alternatively, g_A can be directly obtained from neutron final state decay asymmetries. We employ the lifetime method here, because it is currently more precise.

In the case of muon capture, we have four form factors all evaluated at q_0^2: vector (F_1), induced weak magnetism (F_2), axial-vector (F_A) and induced pseudoscalar (F_P). We define these form factors to all have the same electroweak radiative corrections and explicitly compute those corrections for $F_1(q_0^2)$. Short-distance corrections (which dominate) correspond to a renormalization of the relevant four-fermion operator, and are automatically the same for all form factors. Long distance corrections, although not as important, are incorporated through the form factor definitions in much the same way as g_A is renormalized by definition in neutron decay.

Given the above form factor definitions, their common total radiative correction is conventionally

written as the sum of three terms,

$$\mathrm{RC} = \mathrm{RC(electroweak)} + \mathrm{RC(finite\ size)} + \mathrm{RC(electron\ VP)}\,, \tag{10}$$

which we now specify. Neglecting terms of $\mathcal{O}(E_\ell/m_p, q/m_p)$, where E_ℓ is the charged lepton energy and q the momentum transfer,[5] the radiative corrections to the vector parts of neutron decay and muon capture are of the same form, but evaluated at different q^2 and with different lepton mass. The RC (electroweak) radiative corrections to muon capture [16] were obtained from the original neutron decay calculation, but including higher-order leading log effects denoted by ellipsis in the following Eq. (11):

$$\mathrm{RC(electroweak)} = \frac{\alpha}{2\pi}\left[4\log\frac{m_Z}{m_p} - 0.595 + 2C + g(m_\mu, \beta_\mu = 0)\right] + \cdots = +0.0237(10)\,, \tag{11}$$

where $m_Z = 91.1876\,\mathrm{GeV}$, $m_p = 0.9383\,\mathrm{GeV}$, $C = 0.829$ [41], and $g(m_\mu, \beta_\mu = 0) = 3\log(m_p/m_\mu) - 27/4$ was obtained from Eq. (20b) in Ref. [47] by replacing $m_e \to m_\mu$, ignoring bremsstrahlung and taking the $\beta_\mu = 0$ and $m_\mu/m_p = 0$ limits. The ellipsis in Eq. (11) denotes higher order (in α) corrections enhanced by large logarithms [42]. These effects have been added to the $+2.23\%$ order α correction to obtain the total $+2.37\%$ electroweak radiative correction. The uncertainty has been reduced from 0.4% in Ref. [16] to 0.1%. That reduction is justified by two improvements in the analysis. First, the radiative corrections to V_{ud} (such as C) are correlated with similar corrections in Eq. (11), and their uncertainties largely cancel. Second, (ignoring nuclear structure), direct calculation of $\mathcal{O}(\alpha m_\mu/m_p)$ corrections to muon capture (that were ignored in Ref. [16]) were found to cancel and not contribute to the uncertainty in Eq. (11).

Here, we assume that corrections of $\mathcal{O}(\alpha m_\mu/m_p)$ due to nuclear structure are parametrized by the nucleon finite size reduction factor [48]

$$|\psi_{1\mathrm{S}}(0)|^2 \to \frac{m_r^3\alpha^3}{\pi}\left(1 - 2\,\alpha\, m_r\langle r\rangle\right)\,, \tag{12}$$

where $\langle r\rangle$ denotes the first moment of the proton charge distribution. Based on a range of model forms for this distribution, the correction (12) evaluates to

$$\mathrm{RC(finite\ size)} = -0.005(1)\,, \tag{13}$$

where the error spans the central values -0.0044 [31], -0.005 [16], and -0.0055 [35] given in the literature. We note that the quoted uncertainty may not fully account for possible additional effects of nuclear structure which could be estimated using a relativistic evaluation of the γ-W box diagrams, but are beyond the scope of this article.[6]

The corrections RC(electroweak) and RC(finite size) modify the coefficients c_i of the effective Hamiltonian (4). The remaining radiative correction, from the electron vacuum polarization modification to the muonic atom Coulomb potential, is described by δV_{VP}. This contribution amounts to

$$\mathrm{RC(electron\ VP)} = +0.0040(2), \tag{14}$$

where the very small uncertainty 0.02% is estimated by the difference between $1.73\,\alpha/\pi$ of Ref. [16, 27] and $1.654\,\alpha/\pi$ of Ref. [35].

In Eq. (10), we have defined the total radiative correction to include electroweak, finite size and electron vacuum polarization contributions. In Ref. [16], the finite size correction was treated separately, and "radiative correction" referred to the sum of our RC(electroweak) and RC(electron VP), amounting to $\sim 2.8\%$.

Table 2: Input parameter values used in this paper. See text for discussion.

Symbol	Description	Value	Source/Reference
G_F	Fermi coupling constant	$1.1663787(6)\times10^{-5}\,\mathrm{GeV}^{-2}$	Muon lifetime/PDG [43]
V_{ud}	CKM matrix element	0.97417(18)(10)	Superallowed β decays [40]
f_π	pion decay constant	92.3(1) MeV	PDG [43]
$g_{\pi NN}$	pion nucleon coupling	13.12(10)	[49, 50]
expansion parameters for nucleon charged current form factors			
r_1^2	squared rms radius for F_1	0.578(2) fm^2	n-e, μH, see text
$F_2(0)$	weak magnetic coupling	3.70844	see text
r_2^2	squared rms radius for F_2	0.707(53) fm^2	e-p, e-n, π-N, see text
$g_A \equiv F_A(0)$	axial coupling	1.2749(9)	τ_n, see text
r_A^2	squared rms radius for F_A	0.46(22)fm^2	$\nu - d$ [19]
derived nucleon charged current form factors at q_0^2			
$F_1(q_0^2)$	vector form factor	0.97578(8)	this work
$F_2(q_0^2)$	weak magnetic form factor	3.5986(82)	this work
$\bar{g}_A \equiv F_A(q_0^2)$	axial form factor	1.2503(118)	this work
$\bar{g}_P \equiv \frac{m_\mu}{m_N} F_P(q_0^2)$	pseudoscalar form factor	8.25(25)	this work

2.4 Inputs

The relevant inputs used to compute the capture rate are displayed in Table 2. The Fermi constant G_F is determined from the muon lifetime [39] and its uncertainty is negligible in determining the muon capture rate. The CKM matrix element $|V_{ud}|$ is determined from superallowed β decays [40]. The uncertainty in Table 2 is divided into a nucleus-independent radiative correction term, 0.00018, and a second term 0.00010 representing the sum in quadrature of other theoretical-nuclear and experimental uncertainties. The former radiative correction is strongly correlated with RC(electroweak) in Eq. (11), and the corresponding uncertainty largely cancels when the muon capture rate is expressed in terms of $|V_{ud}|$. This cancellation has been accounted for in our discussion of radiative corrections; in the numerical analysis the uncertainty contribution 0.00018 to $|V_{ud}|$ is dropped.[7]

The charged current isovector vector form factors are obtained from the isovector combination of electromagnetic form factors. Deviations from $F_1(0) = 1$ occur at second order in small isospin violating quantities. At the quark level these quantities may be identified with the quark mass difference $m_u - m_d$ and the electromagnetic coupling α. At the hadron level, isospin violation manifests itself as mass splittings within multiplets, such as isodoublet $m_n - m_p$ and isotriplet $m_{\pi^\pm}^2 - m_{\pi^0}^2$ [44–46]. As shown in Ref.[44], first-order isodoublet mass splitting corrections vanish in $F_1(q^2)$ and $F_2(q^2)$, for general q^2, while first order isotriplet ones cancel in $F_1(0)$ but contribute in $F_1(q^2)$ for $q^2 \neq 0$ and in $F_2(q^2)$ for all values of q^2. Estimating these corrections to be of $\mathcal{O}([m_{\pi^+}^2 - m_{\pi^0}^2]/m_\rho^2) = 2.1 \times 10^{-3}$, where $m_\rho \approx 770\,\mathrm{MeV}$ is the ρ meson mass (representing a typical hadronic mass scale), we note that in $F_1(q_0^2)$ they are accompanied by the further suppression factor $q_0^2\, r_1^2/6 = -2.4\times10^{-2}$, so they amount to -5×10^{-5}. Corrections to the isospin limit in $F_1(q_0^2)$ are thus negligible at the required permille level. In the case of $F_2(q_0^2)$, we note that in the expression for the singlet capture rate [Eq. (20) below], a 2.1×10^{-3} correction to the F_2 term within

[5] For the kinematics of muon capture, $E_\ell/m_p \sim q/m_p \sim m_\mu/m_p$.

[6] The finite size ansatz (12) becomes exact in the large-nucleus limit, $r_{\mathrm{nucleus}} \gg r_{\mathrm{weak}}$, where $r_{\mathrm{nucleus}} \sim r_{E,p}$ is the nuclear (proton) charge radius and $r_{\mathrm{weak}} \in (r_1, r_2, r_A)$ denotes a weak vector or axial radius.

[7] The muon capture rate could be expressed directly in terms of β decay observables, such as the neutron lifetime, where $|V_{ud}|$ does not appear explicitly.

square brackets amounts to 6.67×10^{-4}, while the total contribution from the four form factors is 4.217.[8] Thus, a 2.1×10^{-3} isotriplet mass splitting correction to $F_2(q_0^2)$ induces a $2 \times 6.67 \times 10^{-4}/4.217 = 3.2 \times 10^{-4}$ correction to the singlet capture rate, which is also negligible at the permille level.

Neglecting these small corrections, the Dirac form factor is thus normalized to $F_1(0) = 1$. The Pauli form factor at zero momentum transfer is given by the difference of the proton and neutron anomalous magnetic moments: $F_2(0) = \kappa_p - \kappa_n$, where $\kappa_p = 1.79408$ and $\kappa_n = -1.91436$ are measured in units of $e/2m_N$. This leads to $F_2(0) = 3.70844$. Note that since the PDG [43] expresses both proton and neutron magnetic moments in units of $e/2m_p$, our value for $F_2(0)$ differs from a simple difference of magnetic moments quoted there by a factor $m_N/m_p = 1.00069$.

The q^2 dependence of the form factors is encoded by the corresponding radii, defined in terms of the form factor slopes:

$$\frac{1}{F_i(0)} \frac{dF_i}{dq^2}\bigg|_{q^2=0} \equiv \frac{1}{6} r_i^2 \,. \tag{15}$$

Curvature and higher-order corrections to this linear approximation enter at second order in small parameters $q_0^2/\Lambda^2 \sim m_\mu^2/m_\rho^2$, where Λ is a hadronic scale characterizing the form factor. These corrections may be safely neglected at the permille level. Isospin violating effects in the determination of the radii may be similarly neglected. The Dirac-Pauli basis F_1, F_2 is related to the Sachs electric-magnetic basis G_E, G_M by $G_E = F_1 + (q^2/4m_N^2)F_2$, $G_M = F_1 + F_2$. In terms of the corresponding electric and magnetic radii,[9]

$$r_1^2 = r_{E,p}^2 - r_{E,n}^2 - \frac{3}{2m_N^2} F_2(0) \,, \quad r_2^2 = \frac{1}{F_2(0)} (\kappa_p \, r_{M,p}^2 - \kappa_n \, r_{M,n}^2 - r_1^2) \,. \tag{16}$$

The neutron electric radius is determined from neutron-electron scattering length measurements, $r_{E,n}^2 = -0.1161(22)\,\mathrm{fm}^2$ [43]. The proton electric radius is precisely determined from muonic hydrogen spectroscopy, $r_{E,p} = 0.84087(39)\,\mathrm{fm}$ [2]; this result remains controversial, and is 5.6σ discrepant with the value $r_{E,p} = 0.8751(61)$ obtained in the CODATA 2014 adjustment [51] of constants using electron scattering and ordinary hydrogen spectroscopy. We take as default the more precise muonic hydrogen value, but verify that this $r_{E,p}$ puzzle does not impact the capture rate at the projected 0.33% level. The magnetic radii are less well constrained. We adopt the values $r_{M,p} = 0.776(38)\,\mathrm{fm}$ [43] and $r_{M,n} = 0.89(3)\,\mathrm{fm}$ [52].[10]

Currently, the most precise determination of g_A comes indirectly via the neutron lifetime, τ_n, used in conjunction with $V_{ud} = 0.97417(10)(18)$ obtained from super-allowed nuclear β decays [40–42]. Correlating theoretical uncertainties in the electroweak radiative corrections to τ_n and V_{ud},[11] reduces the uncertainty in Eq. (9) to $1 + 3g_A^2 = 5172.4(1.1)\,\mathrm{s}/\tau_n$.[12] For the PDG average [43], $\tau_n = 880.2(1.0)\,\mathrm{s}$, one finds $g_A = 1.2749(9)$, the value we use throughout this text. That average includes a PDG scale factor of 1.9 which primarily reflects a lifetime disagreement between trapped neutron decays and free neutron beam

[8] The additional suppression may be traced to a factor m_μ/m_N appearing in the coefficients of F_2 relative to F_1 in Eq. (7). A similar power counting applies to the second class form factors, F_S and F_T in Eq. (6), that we have neglected in our analysis.

[9] The isovector form factors can be written in the form $F_i = F_{i,p} - F_{i,n} (i = 1, 2)$, $G_E = G_{E,p} - G_{E,n}$, $G_M = G_{M,p} - G_{M,n}$, where the subscripts p and n refer to the proton and neutron contributions. The electric and magnetic radii are defined analogously to Eq. (15) in terms of the slopes of $G_{E,p}$, $G_{E,n}$, $G_{M,p}$ and $G_{M,n}$. For the neutron, with $G_{E,n}(0) = 0$, $r_{E,n}^2 \equiv 6\, G'_{E,n}(0)$.

[10] This PDG value for $r_{M,p}$ represents the z expansion reanalysis [53] of A1 collaboration electron-proton scattering data [54]. A similar reanalysis of other world data in Ref. [53] obtained $r_{M,p} = 0.914(35)\,\mathrm{fm}$. We verify that this $r_{M,p}$ discrepancy does not impact the capture rate at the projected 0.33% level. For $r_{M,n}$, we adopt the value from the z expansion reanalysis [52] of $G_{M,n}$ extractions, combined with dispersive constraints (see also Ref. [55]). The larger uncertainty encompasses the PDG value, $0.864^{+0.009}_{-0.008}\,\mathrm{fm}$, obtained by averaging with the dispersion analysis of Ref. [56].

[11] The first, 1.8×10^{-4}, uncertainty on $|V_{ud}|$ in Table 2 is correlated with the 1.9 s uncertainty on the right hand side of Eq. (9). These uncertainties cancel.

[12] The formula relating g_A and τ_n [42] is based on a neutron decay phase space factor $f = 1.6887$ (cf. Ref. [57]).

decay in flight [58]. The direct neutron decay asymmetry PDG g_A average [43], 1.2723(23), is lower; but most more recent experiments find values close to 1.276.

Our knowledge about the functional form of $F_A(q^2)$ relies primarily on neutrino-deuteron scattering data from bubble chamber experiments in the 1970's and 1980's: the ANL 12-foot deuterium bubble chamber experiment [59–61], the BNL 7-foot deuterium bubble chamber experiment [62], and the FNAL 15-foot deuterium bubble chamber experiment [63, 64]. As mentioned in the Introduction, the original analyses and most follow-up analyses employed the one-parameter dipole model of the axial form factor. A more realistic assessment of uncertainty allows for a more general functional form. Using a z expansion analysis [19], the uncertainty on the axial radius is found to be significantly larger than from dipole fits,

$$r_A^2(z \text{ exp.}, \nu) = 0.46(22)\,\text{fm}^2\,. \tag{17}$$

This value may be compared to a fit of scattering data to the dipole form, $r_A^2(\text{dipole}, \nu) = 0.453(23)\,\text{fm}^2$ [17]. Note that the value $r_A^2(\text{dipole}) = 0.454(13)\,\text{fm}^2$ quoted in the Introduction is obtained by averaging this neutrino scattering result with an extraction from pion electroproduction [17], $r_A^2(\text{dipole, electro.}) = 0.454(14)\,\text{fm}^2$. As observed in Ref. [18], the electroproduction extraction is also strongly influenced by the dipole assumption. A more detailed discussion of the electroproduction constraints is given in Sec. 5, with the conclusion that further control over systematics is required in order to provide a reliable r_A^2 extraction. The pion decay constant f_π and pion nucleon coupling $g_{\pi NN}$, along with r_A^2, are used to determine the induced pseudoscalar form factor [11]

$$F_P(q_0^2) = \frac{2m_N g_{\pi NN} f_\pi}{m_\pi^2 - q_0^2} - \frac{1}{3}\, g_A\, m_N^2\, r_A^2 + \dots\,, \tag{18}$$

where $m_\pi = 139.571\,\text{MeV}$ is the charged pion mass. Two loop χPT corrections, indicated by the ellipsis in Eq. (18), were estimated to be negligible, as long as the low energy constants involved remain at natural size [13]. f_π is determined from the measured rate for $\pi^- \to \mu^-\bar{\nu}_\mu(\gamma)$, and its uncertainty is dominated by hadronic structure dependent radiative corrections. For $g_{\pi NN}$ we take as default the value $g_{\pi NN} = 13.12(6)(7)(3) = 13.12(10)$ [49, 50], where the first two errors are attributed to pion-nucleon scattering phase shifts and integrated cross sections, respectively, entering the Goldberger-Miyazawa-Oehme (GMO) sum rule for $g_{\pi NN}$. The third error is designed to account for isospin violation and was motivated by evaluating a subset of χPT diagrams. Other values include $g_{\pi NN} = 13.06(8)$ from partial wave analysis of nucleon-nucleon scattering data [65]; and $g_{\pi NN} = 13.14(5)$ [66], $g_{\pi NN} = 13.150(5)$ [67] from partial wave analysis of pion-nucleon scattering data. That range of values is covered by the error given in Table 2.

2.5 Numerical results

Employing the radiative corrections given above, the full capture rates become

$$\Lambda = [1 + \text{RC}]\,\Lambda_{\text{tree}} = [1 + 0.0277(10)(2) - 0.005(1)]\,\Lambda_{\text{tree}}\,, \tag{19}$$

where Λ_{tree} is the tree level expression for the chosen spin state. We have displayed a conventional separation of the radiative corrections in Eq. (19), where the first $+2.8\%$ includes the electroweak and electron vacuum polarization corrections, and the second -0.5% is the finite size correction. Inserting the relevant quantities from Table 2, the singlet 1S capture rate is given by

$$\Lambda_{\text{singlet}} = 40.226(56)\,[F_1(q_0^2) + 0.08833\,F_2(q_0^2) + 2.63645\,\bar{g}_A - 0.04544\,\bar{g}_P]^2\,\text{s}^{-1}\,, \tag{20}$$

where the quantities $\bar{g}_P$ and $\bar{g}_A$ are defined below and the relative uncertainty $u_r = 1.4{\times}10^{-3}$ in the prefactor of Eq. (20) quadratically sums the relative uncertainties $u_r(\text{RC}) = 1.40{\times}10^{-3}$ and $u_r(V_{ud}) =$

0.20×10^{-3}.[13] In the discussion above, we define $u_r = \delta X/X$ as the relative uncertainty in the considered quantity X having an uncertainty δX. The relative uncertainty in X induced by parameter p with uncertainty δp is $u_r(p) = X^{-1}(\partial X/\partial p)\delta p$.

As a next step, we evaluate the form factors at the momentum transfer q_0^2 relevant for muon capture. For the vector form factors, we expand to linear order using Eq. (15),

$$F_1(q_0^2) = 0.97578(8)\,, \quad F_2(q_0^2) = 3.5986(82)\,. \tag{21}$$

For the axial form factor we have

$$\bar{g}_A \equiv F_A(q_0^2) = 1.2503\ (118)_{r_A^2}\ (9)_{g_A} = 1.2503(118)\,, \tag{22}$$

with the uncertainty dominated by $u_r(r_A^2) = 9.4 \times 10^{-3}$. Finally, the pseudoscalar form factor predicted by χPT is

$$\bar{g}_P \equiv \frac{m_\mu}{m_N} F_P(q_0^2) = 8.743\ (67)_{g_{\pi NN}}(9)_{f_\pi} - 0.498\ (238)_{r_A^2}\ = 8.25(25)\,, \tag{23}$$

where the contribution from the pole and higher order term in Eq.(18) are shown separately. While the pole term dominates the value for $\bar{g}_P$, the uncertainty is actually dominated by the non-pole term, due to the rather dramatically increased uncertainty in r_A^2.

We exhibit the sensitivity to the axial form factors by inserting the relatively well known vector form factors in Eq. (20) to obtain

$$\Lambda_{\rm singlet} = 67.318(94)\ \left[1.00000(56) + 2.03801\ \bar{g}_A - 0.03513\ \bar{g}_P\right]^2\ {\rm s}^{-1}\,. \tag{24}$$

At the central values for $\bar{g}_A$ and $\bar{g}_P$, the uncertainty in this equation from the remaining inputs is $\delta\Lambda_{\rm singlet} = 1.03\ {\rm s}^{-1}$, corresponding to a relative error u_r=1.44×10^{-3}, which is still dominated by RC, with a minor contribution from $u_r(F_2)$=0.3×10^{-3}. At this point the traditional approach would be to insert $\bar{g}_A$ and $\bar{g}_P$ in the equation above and to specify the uncertainties in $\Lambda_{\rm singlet}$ arising from these two axial form factors. However, as both $\bar{g}_A$ and $\bar{g}_P$ depend on the axial radius squared r_A^2, which is not well known, they cannot be treated as independent input quantities. To avoid their correlation, we express $\Lambda_{\rm singlet}$ in terms of the independent input parameters (g_A, r_A^2, $g_{\pi NN}$):

$$\Lambda_{\rm singlet} = 67.318(94)\ [1.00000(56) - 0.02341(3)\ g_{\pi NN} + (2.03801 - 0.05556\ r_A^2)\ g_A]^2\ {\rm s}^{-1}\,, \tag{25}$$

with r_A^2 in units of fm^2. Using the current knowledge of these independent input quantities from Table 2, we obtain our best prediction for the muon capture rate in the singlet and triplet hyperfine states of muonic hydrogen as

$$\Lambda_{\rm singlet} = 714.8\ (7.0)\ {\rm s}^{-1}\,, \tag{26}$$

$$\Lambda_{\rm triplet} = 12.09\ (52)\ {\rm s}^{-1}\,. \tag{27}$$

We have employed the same methodology as above for $\Lambda_{\rm singlet}$ to obtain $\Lambda_{\rm triplet}$. The total relative uncertainty for $\Lambda_{\rm singlet}$, $u_r(\Lambda_{\rm singlet}) = 9.8{\times}10^{-3}$, is calculated as the quadratic sum of $u_r({\rm RC}) = 1.4{\times}10^{-3}$, $u_r(g_{\pi NN}) = 1.4{\times}10^{-3}$, $u_r(g_A) = 1.1{\times}10^{-3}$, $u_r(r_A^2) = 9.5{\times}10^{-3}$ and a negligible uncertainty from f_π. Assuming no uncertainty in r_A^2, the prediction for $\Lambda_{\rm singlet}$ would have a more than 4 times smaller error of 1.66 s^{-1}.

3 Muon capture experiment update

Precise measurements of muon capture in hydrogen are challenging, for the following reasons [7, 68]. (i) Nuclear capture takes place after muons come to rest in matter and have cascaded down to the ground

[13] As discussed above, a large part of the uncertainty in V_{ud} cancels with the corresponding uncertainty in radiative corrections to muon capture.

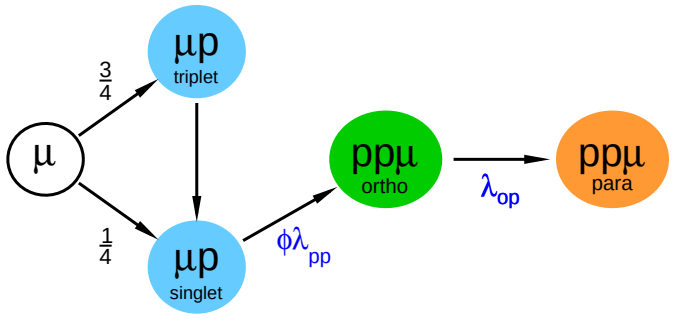

Figure 3: (color online). Reaction sequence after muons stop in hydrogen. Triplet states are quickly quenched to the singlet μH ground state. In collisions, $(pp\mu)$ ortho-molecules are formed proportional to the hydrogen density ϕ and the formation rate λ_{pp}. Ortho-molecules can convert to para-molecules with the poorly-known rate λ_{op}. Reproduced from [7].

state of muonic atoms. As exemplified for the case of μH in Eq. (5), the capture rate is proportional to the square of the muonic wavefunction at the origin,[14] $|\psi_{1S}(0)|^2$, which, after summing over the number of protons in a nucleus of charge Z, leads to a steep increase of the capture rate with $\sim Z^4$, such that the muon capture and decay rates are comparable for $Z \sim$13. For μH, where $Z = 1$, this amounts to a small capture rate of order 10^{-3} compared to muon decay, as well as dangerous background from muon stops in other higher Z materials, where the capture rate far exceeds the one in μH. (ii) On the normal atomic scale μH atoms are small and can easily penetrate the electronic cloud to transfer to impurities in the hydrogen target gas, or to form muonic molecular ions $(pp\mu)^+$. The former issue requires target purities at the part-per-billion level. The latter problem, depicted in Fig. 3, has been a primary source of confusion in the past, as the helicity dependence of weak interactions implies large differences in the capture rates from the possible states. The rates for the two atomic hyperfine μH states are given in Eqs. (26,27), while the molecular rates can be calculated as

$$\Lambda_{\rm ortho} = 544\ {\rm s}^{-1}\ , \tag{28}$$

$$\Lambda_{\rm para} = 215\ {\rm s}^{-1}\ , \tag{29}$$

using the molecular overlap factors given in Eq. (11) of Ref. [7].[15] To interpret a specific experimental capture rate, the fractional population of states for the given experimental conditions has to be precisely known, which is especially problematic for high density targets. (iii) Finally, muon capture in hydrogen leads to an all neutral final state, $n+\nu$, where the 5.2 MeV neutron is hard to detect with well-determined efficiency.

3.1 MuCap experiment: strategy and results

Over the past two decades, the μ^3He experiment, the MuCap and later the MuSun collaboration have developed a novel active target method based on high pressure time projection chambers (TPC) filled with pure ^{3}He, ultra-pure hydrogen (1% of liquid hydrogen (LH_2) density) or cryogenic deuterium gas (6% of LH_2 density), respectively, to overcome the above challenges. The first experiment [71], benefiting from the charged final state, determined the rate for $\mu+^3{\rm He} \to t+\nu$ with an unprecedented precision of 0.3% as $1496.0\pm4.0\,{\rm s}^{-1}$. The most recent extraction [72] of $\bar{g}_P$ from this result gives $\bar{g}_P = 8.2(7)$, with uncertainties

[14] Compare Ref. [69] for corrections relevant for capture and muon-electron conversion in heavy nuclei.

[15] We do not estimate uncertainties for the molecular rates, as a reliable error evaluation at the permille level should include a modern confirmation of the original calculation of the $(pp\mu)^+$ space and spin structure [70].

due to nuclear structure theory. Additional uncertainties would enter if the new $r_A^2(z\text{ exp.},\ \nu)$ is taken into account.[16]

MuCap measured Λ_{singlet} in the theoretically clean μH system to extract $\bar{g}_P$ more directly. The original publication [14] gave $\Lambda_{\text{singlet}}^{\text{MuCap}} = (714.9 \pm 5.4_{\text{stat}} \pm 5.1_{\text{syst}})\ \text{s}^{-1}$, which was slightly updated based on an improved determination of the $(pp\mu)$ molecular formation rate λ_{pp} [15] to its final value

$$\Lambda_{\text{singlet}}^{\text{MuCap}} = (715.6 \pm 5.4_{\text{stat}} \pm 5.1_{\text{syst}})\ \text{s}^{-1}\,. \tag{30}$$

The scientific goal of MuSun [7, 73] is the determination of an important low energy constant (LEC), which characterizes the strength of the axial-vector coupling to the two-nucleon system and enters the calculation of fundamental neutrino astrophysics reactions, like pp fusion in the sun and νd scattering in the Sudbury Neutrino Observatory [74].

As muon capture involves a characteristic momentum transfer of the order of the muon mass, extractions of form factors and LECs from all of these experiments are sensitive to the modified theoretical capture rate predictions or uncertainties implied by the use of the new $r_A^2(z\text{ exp.},\ \nu)$.

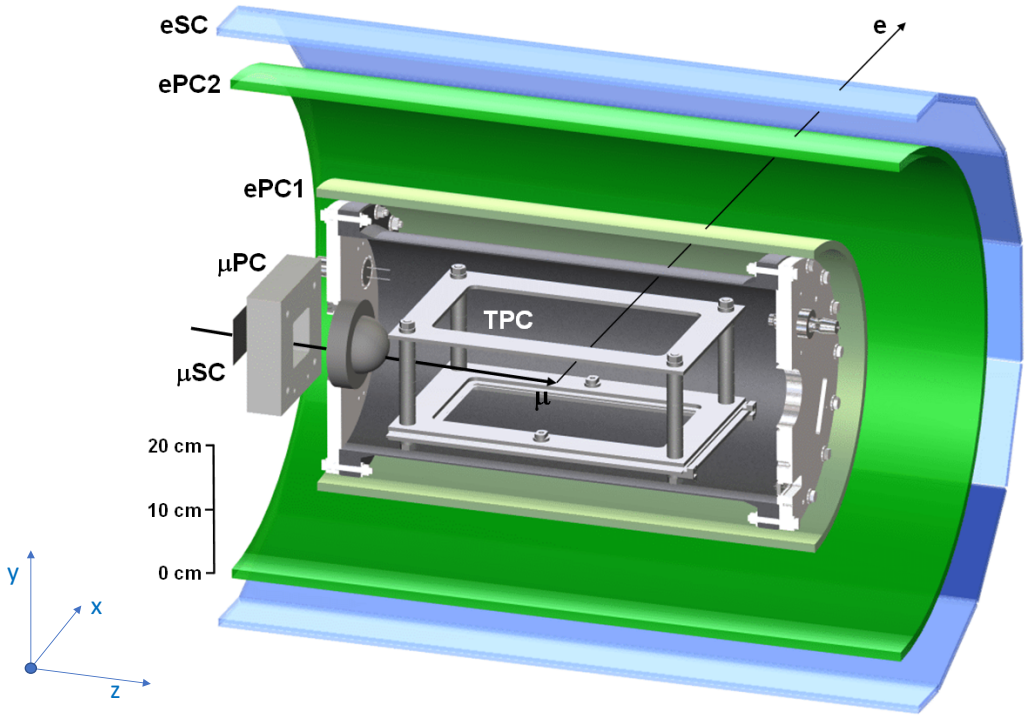

Figure 4: (color online) Simplified MuCap detector model. Reproduced from [29].

In view of potential further improvements, let us analyze in some detail how MuCap achieved its high precision 1% measurement. Fig. 4 illustrates the basic concept. Muons are detected by entrance detectors, a 500-μm thick scintillator (μSC) and a wire chamber (μPC), and pass through a 500-μm-thick hemispherical beryllium pressure window to stop in the TPC, which is filled with ultrapure, deuterium-depleted hydrogen gas at a pressure of 1.00 MPa and at ambient room temperature. Electrons from muon decay are tracked in two cylindrical wire chambers (ePC, green) and a 16-fold segmented scintillator array (eSC, blue). The experimental strategy involves the following key features.

Low density and suppressed $pp\mu$ formation: As the target has only 1% of liquid hydrogen density, molecule formation is suppressed and 97% of muon capture occurs in the μH singlet atom, providing

[16] We refrain from updating this result with new form factors. As the calculation uses tritium decay as input, changes in form factors at q^2=0 are expected to cancel, but the uncertainty in the momentum dependence enters via r_A^2.

unambiguous interpretation of the signal.

Lifetime method [75]: The observable is the disappearance rate λ_- of negative muons in hydrogen, given by the time between muon entrance and decay electron signal. The capture rate is extracted as the difference $\Lambda_{\rm singlet} \approx \lambda_- - \lambda_+$, where λ_+ is the precisely known positive muon decay rate [39]. Contrary to the traditional method of detecting capture neutrons from process (1) which requires absolute efficiencies, only precise time measurements are needed, albeit at large statistics.

Selection of muon stops in hydrogen by tracking: The TPC [76] tracks the incident muons in three dimensions to accept only hydrogen stops sufficiently far away from wall materials with higher capture rate. Its sensitive volume is $15 \times 12 \times 28$ cm^3, with an electron drift velocity of 5.5 mm/μs at a field of 2 kV/cm in vertical y-direction. The proportional region at the bottom of the chamber was operated at a gas gain of 125 – 320, with anode (in x-direction) and cathode (in z-direction) wires read out by time-to-digital converters using three different discriminator levels.

Ultra-pure target gas: Target purity of ~ 10 ppb was maintained with a continuous circulation and filter system [77]. The TPC allowed in-situ monitoring of impurities by observing charged nuclear recoils from $\mu^- + {\rm O} \to \nu_\mu + {\rm N}^*$, in the rare ($\approx 10^{-6}$) cases of muon transfer to impurities. Isotopically pure protium was produced onsite [78] and verified by accelerator mass spectroscopy [79]. In total, 1.2×10^{10} decay events were accepted with muons stopping in the selected restricted fiducial volume.

3.2 Conceptual ideas towards a 3-fold improved muon capture experiment

The 3-fold uncertainty reduction over MuCap implies a precision goal of $\delta\Lambda_{\rm singlet} \sim 2.4\,{\rm s}^{-1}$ which, for definiteness, we assume equally shared between $\delta\Lambda_{\rm singlet}({\rm stat}) = \delta\Lambda_{\rm singlet}({\rm syst}) = 1.7$ s^{-1}. Achieving this goal is no small feat, and we hope that the motivation for a low-q^2 measurement of the axial form factor outlined in this paper will stimulate further innovative experimental ideas. However, in the remainder of this section we follow the more conservative approach to consider incremental improvements to the MuCap strategy only. We note that MuCap was a pioneering experiment developing a new technology, so it is likely that a next generation experiment can be further optimized, based on the lessons learned.

3.2.1 Statistics

A reduction of the 5.4 s^{-1} MuCap statistical uncertainty to 1.7 s^{-1} requires about a 10-fold increase in statistics. Typically, such order of magnitude advances in nuclear/particle physics experiments require concerted upgrades in beam and detector performance.

MuCap accepted only events with a single muon entering the TPC separated from neighboring muons by at least $T_{\rm obs} = 25$ μs. This eliminated combinatorial distortions to the measured time spectra. In the PSI continuous beam with a rate R_μ, the rate for those single muon events would be $R_\mu e^{-R_\mu 2\,T_{\rm obs}}$ only, which is limited to roughly 7 kHz. Thus a muon-on-request scheme was developed (c.f. Fig. 4): A muon in the beam scintillator μSC triggered a fast kicker [80], which deflects the beam for the measuring period $T_{\rm obs}$ to avoid muon pile-up. With $R_\mu = 65$ kHz, μSC had a pile-up free rate of 22 kHz, of which a fraction $\epsilon_{\rm fid} \approx 0.3$ stopped in the fiducial volume of the TPC selected for physics analysis. Including the electron detection efficiency of $\epsilon_e = 0.5$ and deadtime losses, the rate for accepted events was $R_{\rm acc} \sim 2$ kHz.

To increase this rate, it is certainly worthwhile to explore whether the experiment could run with multiple muons in the TPC. If this idea leads to unacceptable systematic complications, the single muon concept could still be preserved by increasing the muon stopping efficiency from $\epsilon_{\rm fid} = 0.3 \to 0.9$ and the electron detection efficiency $\epsilon_e = 0.5 \to 0.7$, together with supplemental improvements in data taking efficiency. The resulting rate increase of about 4.5 yields $R_{\rm acc} \sim 9$ kHz, so that 12×10^{10} events can be collected in 6 months of data taking (including typical up-time fractions for beam and experiment).

We consider 3 main upgrades to reach this goal. i) Minimize any material traversed by the muon beam, so that the beam momentum can be decreased from 34 MeV/c to 29 MeV/c, which reduces the

muon range by nearly a factor 2.[17] Since longitudinal range straggling, as well as part of the transverse expansion of the beam, scales with the total range, a much more compact stopping volume can be realized. The evacuated muon beam pipe should be directly connected to the TPC entrance flange, with the beam detectors reduced to a 200 μm-thin μSC operating in vacuum with modern silicon photomultiplier (SiPM) technology and the Be window diameter reduced, so that it can be made thinner. The beam to air windows and the wire chamber are eliminated, the latter replaced by a retractable beam spot monitor, which is only used during beam tuning and for systematic studies, but does not add material during production data taking. The beam pipe should be designed as a safety containment volume in case of a breach of the Be window, by placing an additional thin window or fast interlock in an upstream focus. In the first focus downstream of the kicker, another thin scintillator might serve as the beam trigger to minimize kicker delay. ii) With a collimated beam impinging on μSC and the detector itself positioned as close as possible to the TPC, a stopping efficiency $\epsilon_{\rm fid}$ approaching unity can be expected for muons seen by this detector. iii) As the beam rate for negative muons drops steeply with momentum, more powerful PSI beams, existing or under development, should be considered.

3.2.2 Systematics

An uncertainty goal of $\delta\Lambda_{\rm singlet}({\rm syst}) = 1.7\ {\rm s}^{-1}$ implies that the negative muon decay rate λ_- in hydrogen has to be measured at least at a precision of 3.7 ppm relative to muon decay. This poses unprecedented requirements on the TPC track reconstruction, as no early to late effects over the measuring interval $T_{\rm obs}$ distorting the decay spectrum are allowed at this level. The main systematic corrections enumerated in Table II of Ref. [14] can be grouped into 4 distinct classes:

i) Boundary and interference effects: By definition, for an infinite TPC no boundary effects (like wall stops, scattering and diffusion) would occur. Interference effects, on the other hand, are generated by decay electrons, affecting the muon stop reconstruction in a time dependent manner. The experiment has to balance these two competing systematic effects, by carefully selecting muons within a clean fiducial volume, without introducing interference distortions. For the final, best MuCap run R07 their total uncertainty added up to $\delta\Lambda_{\rm singlet} = 3.3\ {\rm s}^{-1}$. The obvious remedy for boundary effects is a larger TPC volume, coupled with potential geometry improvements, as well as the reduction in the beam stopping volume. While the dimensions perpendicular to the TPC drift field are only constrained by practical considerations, the drift time cannot be much longer than $T_{\rm obs}$, in order to avoid reducing the acceptable beam rate. We expect that the TPC can be operated with drift fields up to 10 kV/cm, as demonstrated at higher density in MuSun [82], which would double the drift velocity and allow drift distances of 20 cm. To improve the tracking quality, a geometry of independent pads like MuSun has proven advantageous, as the MuCap cathode wires strung in the direction of the muon tracks provide very limited information. As MuSun demonstrated, full digitization of all signals instead of simple threshold timing information, adds powerful tracking capabilities.

ii) Gas impurities: For the R07 run, transfer to gas impurities amounted to $\delta\Lambda_{\rm singlet} \sim 1\ {\rm s}^{-1}$. Gold coating of inner vessel surfaces, improved gas chromatography (already achieved in MuSun) and/or spectroscopy and, most importantly, full digital readout of the TPC signals [82], for in-situ detection of capture recoils, should reduce this uncertainty to below $0.1\ {\rm s}^{-1}$.

iii) Electron detector effects: A significant uncertainty of $\delta\Lambda_{\rm singlet} \sim 1.8\ {\rm s}^{-1}$ was included in the MuCap error budget, because of incompletely understood discrepancies between alternative electron track definitions. Because diffusion processes in hydrogen introduce systematic problems when applying tight vertex cuts, MuCap concluded that precision tracking is not essential. Thus a new experiment should use scintillators or scintillating fibers with SiPM readout, which are simple, robust and more stable than the wire chambers used in MuCap. Then an instrumental uncertainty below 1 ppm similar to MuLan [39] can be expected.

[17] This strong impact of the muon momentum p on its range R follows from the approximate relation $R \propto p^{3.6}$, which can be understood from integrating the Bethe-Bloch energy loss equation, c.f. III.20 of [81].

iv) $pp\mu$ molecular effects: Although capture from $pp\mu$ molecules amounts only to 3% in 1 MPa hydrogen gas, the uncertainty introduced by the inconsistent determinations of the ortho-para rate $\lambda_{\rm op}$ [7] shown in Fig. 3, introduces a $\delta\Lambda_{\rm singlet} \sim 1.8$ s^{-1} uncertainty [15]. As shown in Fig. 2 of Ref. [14], the poor knowledge of $\lambda_{\rm op}$ also leaves unresolved the question whether the previous measurement of ordinary muon capture in liquid hydrogen [75] or, alternatively, the measurement of radiative muon capture [8] strikingly deviates from theory. The high density cryogenic TPC developed for the MuSun μD experiment, could settle both issues with a first precise measurement of $\lambda_{\rm op}$ when filled with protium gas of about 10% liquid density.

Finally, it should be mentioned that the MuCap TPC occasionally suffered sparking issues, which required running with reduced voltage. Better stability and higher gain should be achieved by starting some R&D efforts with smaller prototypes, with improvements to the classical proportional wire chamber technique used by MuCap as well as tests of — now mature — micro-pattern chamber alternatives, like GEMS and micro-megas.

4 Results and opportunities

Having reviewed the status of theory and explored the reach for experiment, in this section we evaluate how well the nucleon form factors and coupling constants can be determined by the present MuCap experiment at 1% precision, and by a potential new experiment at the 0.33% level.

4.1 Updated value for the pseudoscalar coupling $\bar{g}_P$ and extraction of $g_{\pi NN}$

We begin our applications by using the final MuCap experimental result, $\Lambda_{\rm singlet}^{\rm MuCap} = 715.6(7.4)$ s^{-1}, together with our updated $\Lambda_{\rm singlet}^{\rm theory}$ in Eq. (24), to extract a value for $\bar{g}_P$ that can be compared with the prediction of χPT. Both the experimental value and theoretical prediction depend on r_A^2. To illustrate that dependence, we start with the traditional value of $r_A^2({\rm dipole},\ \nu) = 0.453(23)$ fm^2 obtained from dipole fits to neutrino scattering data with a very small ($\sim 5\%$) uncertainty. It leads to:

$$\bar{g}_P{}^{\rm MuCap}\big|_{r_A^2=0.453(23)\,{\rm fm}^2} = 8.22\ (48)_{\rm exp}\ (9)_{\bar{g}_A}\ (6)_{\rm RC} = 8.22(49)\,, \qquad \bar{g}_P{}^{\rm theory} = 8.256(72)\,. \tag{31}$$

For comparison, we take the ratio and find $\bar{g}_P{}^{\rm theory}/\bar{g}_P{}^{\rm MuCap} = 1.00(6)$, which exhibits very good agreement at the $\pm 6\%$ level. Alternatively, employing the more conservative z expansion value obtained from neutrino scattering, $r_A^2(z\ {\rm exp.},\ \nu) = 0.46(22)$ fm^2, with its nearly 50% uncertainty, one finds:

$$\bar{g}_P{}^{\rm MuCap}\big|_{r_A^2=0.46(22)\,{\rm fm}^2} = 8.19\ (48)_{\rm exp}\ (69)_{\bar{g}_A}\ (6)_{\rm RC} = 8.19(84)\,, \qquad \bar{g}_P{}^{\rm theory} = 8.25(25)\,. \tag{32}$$

The uncertainties are considerably larger. However, taking the ratio and accounting for correlated errors, $\bar{g}_P{}^{\rm theory}/\bar{g}_P{}^{\rm MuCap} = 1.01(8)$. Agreement is still very good and theory is tested at about $\pm 8\%$, not a significant loss of sensitivity. If r_A^2 could be independently determined with high precision (for example, using lattice gauge theory techniques), then a new MuCap experiment with a factor of 3 improvement would test χPT at about the 2% level.

Alternatively, the measured capture rate in conjunction with the theoretical formalism can be used to determine the pion-nucleon coupling $g_{\pi NN}$ from the μH atom. This approach is closely related to the extraction of the pseudoscalar form factor, as $g_{\pi NN}$ appears as the least well known parameter in the PCAC pole term of Eq. (18). For this purpose Eq. (24) was recast in terms of the independent parameters ($g_{\pi NN}$, g_A and r_A^2) into Eq. (25), avoiding the correlation between the axial form factors introduced by r_A^2. That prescription gives, for $r_A^2 = 0.46(22)$ fm^2:

$$g_{\pi NN}^{\rm MuCap} = 13.04\ (72)_{\rm exp}\ (8)_{g_A}\ (67)_{r_A^2}\ (10)_{\rm RC} = 13.04(99)\,, \qquad g_{\pi NN}^{\rm external} = 13.12(10)\,. \tag{33}$$

The result is in very good agreement with the external $g_{\pi NN}$ obtained from pion-nucleon phase shift and scattering cross section data, such as the value given in Table 2. It provides a direct 8% test of χPT essentially the same as indirectly obtained from the $\bar{g}_P$ analysis given above. As in the case of $\bar{g}_P$, a future factor of 3 improvement in the capture rate combined with an independent precise determination of r_A^2 would determine $g_{\pi NN}$ to 2%.

4.2 Determination of r_A^2 from muon capture

The basic premise of this paper has been that the error on r_A^2 extracted from neutrino scattering data is much larger (by about an order of magnitude) than generally assumed. Indeed, the value [19] $r_A^2(z \text{ exp. } \nu) = 0.46(22)$ fm^2, based on the z expansion method, that we employed, has a nearly 50% uncertainty. As we shall see in Sec. 5, this is problematic for predicting quasi-elastic neutrino scattering cross sections needed for next-generation neutrino oscillation studies. For that reason, it is timely and useful to consider alternative ways of determining r_A^2. Various possibilities are discussed in Sec. 5; however, first we consider existing and possible future implications from the MuCap experiment.

Muon capture provides a unique opportunity to determine r_A^2, highly complementary to neutrino charged-current scattering. The momentum transfer q_0^2 is small and well defined, rendering higher terms in the q_0^2 Taylor expansion negligible. However, the effect of r_A^2 is small, with $F_A(q_0^2)$ being only $r_A^2\, q_0^2/6 \approx 2\%$ smaller than $F_A(0)$. Thus precision experiments at the sub-percent level are called for.

The change in Λ_{singlet} due to a change in r_A^2 is given in Eqs. (24),(25), and can be quantified as

$$\frac{\partial \Lambda_{\text{singlet}}}{\partial r_A^2} = \frac{\partial \Lambda_{\text{singlet}}}{\partial \bar{g}_A}\frac{\partial \bar{g}_A}{\partial r_A^2} + \frac{\partial \Lambda_{\text{singlet}}}{\partial \bar{g}_P}\frac{\partial \bar{g}_P}{\partial r_A^2} = -47.8 + 16.7 = -31.1 \text{ s}^{-1} \text{ fm}^{-2} \,. \tag{34}$$

Thus, a one sigma step of 0.22 fm^2 in r_A^2 changes Λ_{singlet} by 6.8 s^{-1} or about 1%. Unfortunately, for the present purpose, the sensitivity to the axial radius is reduced, as the contributions from $\bar{g}_A$ and $\bar{g}_P$ counteract.

Employing Eq.(25) with the input from Table 2 we find

$$r_A^2(\text{MuCap}) = 0.43\ (24)_{\text{exp}}\ (3)_{g_A}\ (3)_{g_{\pi NN}}\ (3)_{\text{RC}} = 0.43(24) \text{ fm}^2. \tag{35}$$

This result is comparable in uncertainty to the z expansion fit to the pioneering neutrino scattering experiments [19]. Making the reasonable assumption that the two approaches are uncorrelated, we can compute the weighted average

$$r_A^2(\text{ave.}) = 0.45(16) \text{ fm}^2. \tag{36}$$

The averaged uncertainty has been reduced to about 35%. A future experiment, assumed to reduce the overall MuCap error from 1% to 0.33% would reduce the error in r_A^2 to

$$\delta r_A^2(\text{future exp.}) = (0.08)_{\text{exp}}\ (0.03)_{g_A}\ (0.03)_{g_{\pi NN}}\ (0.03)_{\text{RC}} = 0.10 \text{ fm}^2. \tag{37}$$

The muon capture squared axial radius determination, when averaged with the neutrino scattering z expansion result, would then have about a 20% uncertainty. This precision level is important, as it would be sufficient to reduce the r_A^2 dependent theoretical uncertainty in neutrino quasielastic cross sections to a subdominant contribution, as we demonstrate below in Sec. 5.1.

4.3 Determination of g_A and electron-muon universality

The axial coupling governing neutron β decay, $g_A = F_A(0)$, is a critically important QCD induced physics parameter [83]. Taken together with the neutron lifetime, τ_n, it can provide a clean determination of V_{ud} free of nuclear physics uncertainties, via Eq. (9). In addition, g_A is needed for constraining the number of effective neutrino species from primordial nucleosynthesis; computing reactor and solar neutrino fluxes and cross-sections; parametrizing the proton spin content and testing the Goldberger-Treiman relation [84].

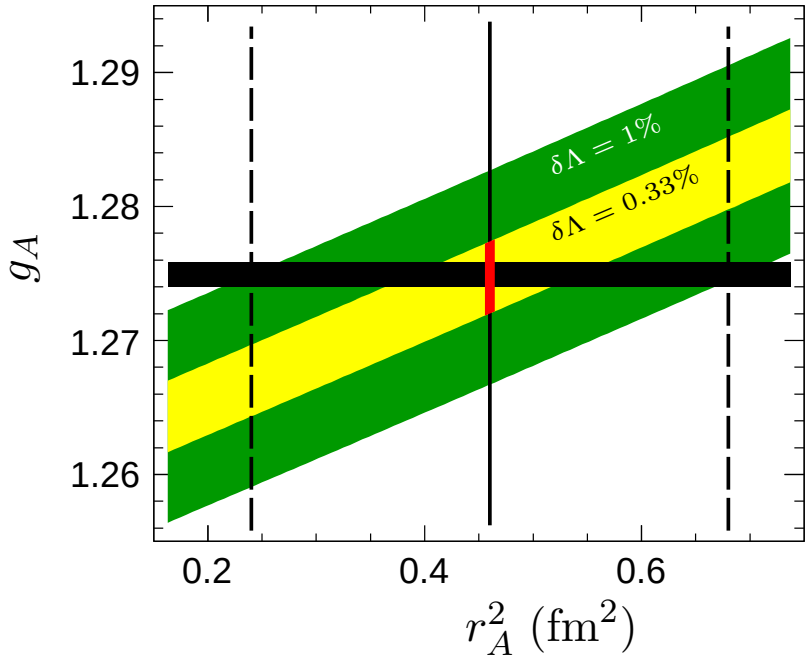

Figure 5: (color online) Relation between g_A and r_A^2 from electron and muon processes. The black band shows g_A from neutron β decay (Table 2). The green band denotes the $g_A - r_A^2$ region consistent with the present MuCap result within 1-sigma, the yellow band the potential of a future 3-times improved measurement (the same central value has been assumed). The current value and uncertainty in r_A^2 from the neutrino scattering analysis is shown by vertical lines. If r_A^2 would be known to 1%, the future experiment would determine g_A within the red region.

In this paper we use the value $g_A = 1.2749(9)$, based on the PDG value for τ_n and V_{ud} given in Table 2. We should note, however, that a recent trapped neutron lifetime experiment at Los Alamos [85] with very small systematic uncertainties finds $\tau_n = 877.7(7)\,\mathrm{s}$, in strong support of earlier trapped neutron results. Roughly estimating the effect of the new result on the neutron lifetime average suggests a preliminary average $\tau_n^{\mathrm{ave.}} = 879.3(9)\,\mathrm{s}$. This shorter average lifetime leads to a larger $g_A = 1.2757(7)$ which is very consistent with the most recent direct neutron decay asymmetry measurements of g_A [43]. Of course, a larger g_A used as input will lead to a larger $\bar{g}_P{}^{\mathrm{MuCap}} = 8.24(84)$, but one still fully consistent with theory, $\bar{g}_P{}^{\mathrm{theory}} = 8.25(25)$. The error on g_A is expected to be further reduced to about $\pm 0.01\%$, by future τ_n and direct neutron decay asymmetries. It will be interesting to see if the two methods agree at that level of precision.

For now, the value of r_A^2 obtained from the z expansion fit to neutrino-nucleon quasi-elastic scattering together with the MuCap singlet muonic Hydrogen capture rate $\Lambda_{\mathrm{singlet}}^{\mathrm{MuCap}}$ can be used in Eq. (25) to obtain a muon based value, $g_A = 1.276(8)_{r_A^2}(8)_{\mathrm{MuCap}} = 1.276(11)$. That overall roughly $\pm 1\%$ sensitivity is to be compared with the current, better than $\pm 0.1\%$, determination of g_A from the electron based neutron lifetime that we have been using in our text, or the preliminary update including Ref. [85] given above. The good agreement can be viewed as a test of electron-muon universality in semileptonic charged current interactions at roughly the 1% level. We have described how a factor of 3 improvement in the MuCap capture rate may be experimentally feasible. A similar factor of 3 or even much better improvement in r_A^2 seems possible from lattice QCD first principles calculations. Together, such advances would provide

a muon based determination of g_A to about $\pm 0.2 - 0.3\%$ and thereby test electron-muon universality via g_A at about a factor of 4 better than currently constrained. Such a comparison is graphically illustrated in Fig. 5 where the current electron determination of g_A from the neutron lifetime is represented by the narrow horizontal band. (A shift in the neutron lifetime would displace the band up or down.) Muon capture constraints depend on r_A^2 and the singlet capture rate as illustrated by the vertical dashed lines and shaded sloped bands.

5 Towards a more precise r_A^2

The momentum dependence of nucleon form factors is critical in many physical processes. The various nucleon radii, defined for each form factor analogously to Eq. (2), parameterize this momentum dependence at low q^2. In fact, for momentum transfers $|q^2| \lesssim$ few GeV^2, the form factors become approximately linear functions in the z expansion: Even in the high-statistics datasets for electromagnetic form factors, the curvature and higher order coefficients of the z expansion are only marginally different from zero [55]. This emphasizes the prominence of the form factor charges (i.e., normalizations at $q^2 = 0$) and radii (i.e., slopes at $q^2 = 0$).[18] In a nonrelativistic picture, the form factor radii can be interpreted in terms of nucleon structure. For example, the electric charge form factor of the proton represents the Fourier transform of the proton charge distribution, and r^2 is readily identified as a mean-square radius in this picture. Similarly, the isovector axial form factor can be interpreted as the Fourier transform of a spin-isospin distribution within the nucleon. Independent of intuitive nonrelativistic models, the form factor charges and radii systematically describe the response of nucleons to weak and electromagnetic probes.

Since the form factors are approximately linear over a broad q^2 range, the radii constrain (and can be probed by) a variety of processes. For example, the proton charge radius that is probed at ∼eV energy scales using hydrogen spectroscopy can be compared with measurements at ∼GeV energy scales using elastic electron-proton scattering. Similarly, constraints on the axial radius from low-energy muon capture translate to constraints on higher-energy neutrino scattering processes. In Sec. 5.1 below, we highlight an important application to quasielastic neutrino scattering and the precision neutrino oscillation program.

The current uncertainty on r_A^2 from is about 50%. In this paper, we have shown that the MuCap experiment already provides similar sensitivity and a future factor of 3 improvement in a MuCap like experiment could lead to a roughly 20% determination of r_A^2. In Sec. 5.2, we address the capability of other approaches to the precise determination of r_A^2. As we shall see, currently, it seems that dedicated lattice studies and neutrino scattering experiments offer the best opportunities.

5.1 Impact of improved r_A^2 on accelerator neutrino cross sections

The discovery of neutrino masses, mixing and oscillations provides our first real indication of "new physics", beyond Standard Model expectations. The source of those effects is likely to arise from very short-distance phenomena that may require new technologies and high energy colliders to unveil. However, in the meantime, improvements in neutrino oscillation measurements can still provide important new discoveries. In that regard, ongoing and proposed neutrino oscillation experiments will address the following questions: Is CP violated in neutrino mixing? Are the neutrino masses ordered in magnitude in the same or different way than their charged lepton counterparts? Do neutrinos have additional interactions with matter that can be explored through neutrino oscillation interferometry? Answers to those questions could help explain the source of the matter-antimatter asymmetry of our universe, a deep fundamental mystery tied to our very existence.

Neutrino-nucleus interaction cross sections at GeV energies are critical to extracting fundamental neutrino properties and parameters from long baseline oscillation experiments [87–89]. Uncertainties in these cross sections arise from the elementary nucleon level scattering amplitudes, and from data-driven

[18] The $|q^2| \lesssim$ few GeV^2 regime encompasses many physics applications. At larger momentum transfers, inelastic processes compete with the elastic process that is determined by the form factors. For a discussion of $F_A(q^2)$ at large $|q^2|$ see Ref. [86].

nuclear modeling for detectors consisting of carbon, water, argon, etc. [90–92]. A typical oscillation experiment employs a "near" detector, close to the production source of neutrinos, and a "far" detector, located at a sufficiently large distance to allow for observable oscillations. Naively, the near-far detector comparison can be used to avoid reliance on neutrino interaction cross sections. However, a number of effects do not cancel in this comparison: flux differences between near and far (e.g. due to oscillation effects and neutrino beam divergence); flavor dependence of cross sections (e.g. the near detector may constrain ν_μ cross sections, whereas the far detector may search for ν_e appearance signal); and degeneracies between errors in neutrino energy reconstruction from undetected particles (such as neutrons, and other sub-threshold particles) and errors from neutrino interaction uncertainties [92].

At the nucleon level, the q^2 dependence of the axial form factor is an important source of uncertainty. This uncertainty directly impacts the final cross section, but also complicates the validation of nuclear, flux, and detector modeling, all of which are predicated on quantitatively understanding the simplest quasielastic process. As an example, the MiniBooNE [20] analysis of quasielastic neutrino-carbon scattering data yielded $r_A^2(\text{MiniBooNE}) = 0.26(7)\ \text{fm}^2$, in tension with historical values obtained from neutrino-deuteron scattering data. Without quantitative control over the nucleon-level amplitudes it is not possible to unambiguously identify the source of the discrepancy.

As a proxy for the relevant class of neutrino observables, let us consider the quasielastic neutrino-neutron cross section at neutrino energy $E_\nu = 1\,\text{GeV}$. Assuming the dipole ansatz for $F_A(q^2)$, with [17] $r_A^2(\text{dipole}) = 0.454(13)\,\text{fm}^2$, this cross section may be evaluated as[19]

$$\sigma_{\nu n\to\mu p}(E_\nu = 1\,\text{GeV},\,\text{dipole}) = 10.57(14)\times 10^{-39}\,\text{cm}^2\,, \tag{38}$$

where for the present illustration, we neglect uncertainties from sources other than $F_A(q^2)$, such as radiative corrections and vector form factors. Using instead the z expansion representation of $F_A(q^2)$ in Ref. [19], the result is

$$\sigma_{\nu n\to\mu p}(E_\nu = 1\,\text{GeV},\,z\text{ exp.}) = 10.1(9)\times 10^{-39}\,\text{cm}^2\,, \tag{39}$$

i.e., an uncertainty of order 10%, an order of magnitude larger than the uncertainty obtained from the corresponding dipole prediction.

In order to illustrate the impact of improved constraints on r_A^2, we begin by reproducing the fits of Ref. [19], using in addition to the neutrino-deuteron scattering data, an external constraint on r_A^2 (coming, e.g. from muon capture). The results are displayed in Fig. 6. Here we first compare the reference fit to a fit where the slope ($\propto r_A^2$) is constrained to a particular value (chosen for illustration as the central value $r_A^2 = 0.46\,\text{fm}^2$ of the reference fit). The yellow band in the figure represents the cross section uncertainty that would result from an external radius constraint with negligible error. As we noted above, $F_A(q^2)$ becomes approximately linear when expressed as a Taylor expansion in z, in the sense that curvature in z and higher order z expansion coefficients, are consistent with zero, within errors [19]. However, these coefficients, when varied over their allowed range, contribute to the error budget, represented by the width of the yellow band in the figure.

To illustrate the impact of a finite uncertainty on the external radius constraint, we recompute the cross section using an external radius constraint that differs by ±20% from the chosen central value (recall that this corresponds to the level of precision on r_A^2 attainable by a future 0.33% muon capture rate measurement). This variation is represented by the black hatched band in the figure. The uncertainties represented by the yellow and hatched bands should be added in quadrature to obtain the total cross section error. At an illustrative $E_\nu = 1\,\text{GeV}$, the result is summarized by

$$\sigma_{\nu n\to\mu p}(E_\nu = 1\,\text{GeV},\,z\text{ exp.}) = 10.2 \pm 0.47 \pm \left(0.28\frac{\delta r_A^2/r_A^2}{20\%}\right)\times 10^{-39}\,\text{cm}^2\,. \tag{40}$$

[19] For definiteness we employ the remaining parameter and form factor choices of Ref. [19].

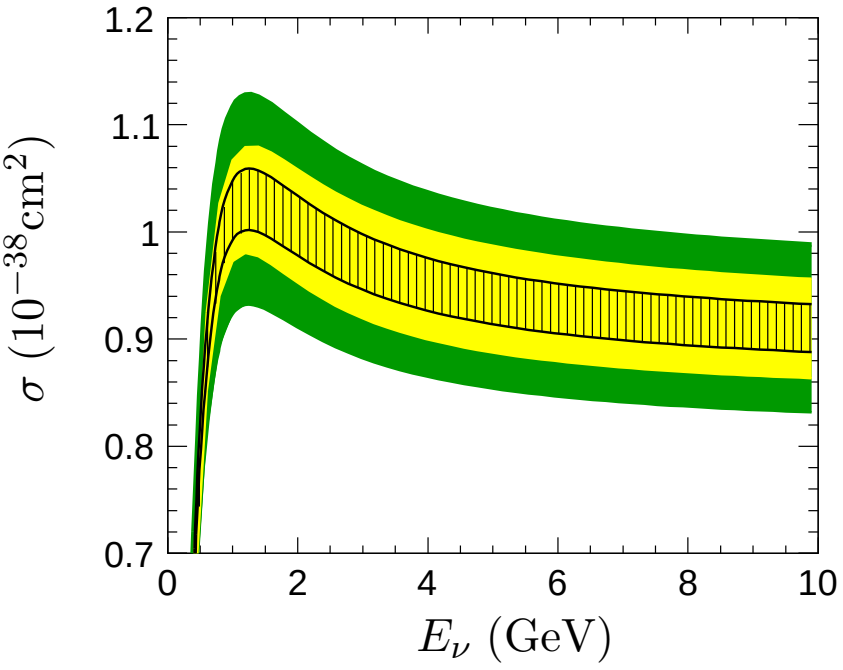

Figure 6: (color online) Quasielastic neutrino-neutron cross section. Reference fit of Ref. [19] in green band shows the current uncertainty. The yellow band shows the uncertainties independent of r_A^2. The hatched black band shows the uncertainty contribution from r_A^2, if r_A^2 would be known to 20% (using the central value from the reference fit). In that case, the r_A^2 contribution would be subdominant in the total error (quadratic sum of yellow and black hatched), as illustrated at $E_\nu = 1\,\mathrm{GeV}$ in Eq. (40).

External constraints on r_A^2, used in conjunction with the existing deuteron target neutrino scattering data, can thus lead to a halving of the uncertainty on the elementary signal cross section for long baseline neutrino experiments. Advances in our quantitative understanding of neutrino scattering, through improvements in r_A^2, heavy nuclear target modeling and direct precise neutrino cross-section measurements will allow us to fully exploit the planned sensitivity of future oscillation experiments.

5.2 Other constraints and applications

Given the importance of r_A^2, and more generally $F_A(q^2)$, let us understand what complementary information exists from other approaches. This information comes from theoretical approaches to determine $F_A(q^2)$ from the QCD Lagrangian; and from experimental measurements using weak and electromagnetic probes of the nucleon.

5.2.1 Lattice QCD

Lattice QCD is a computational method for determining low energy properties of hadrons based on first principles starting from the QCD Lagrangian.[20] This method has reached a mature state for meson properties.[21] Nucleons present an additional challenge for lattice simulations, owing to a well-known noise problem [94]. A variety of approaches are being taken to explore and address the simultaneous

[20] For a brief introduction and references see the lattice QCD review of S. Hashimoto, J. Laiho and S. R. Sharpe in Ref. [43].
[21] For a review and further references, see Ref. [93].

challenges of excited states, lattice size, finite volume, as well as statistical noise. In many cases, the need to extrapolate from unphysically large light quark masses is overcome by performing the lattice calculation at (or near) the physical masses. Background field and correlator derivative techniques are being explored to optimize the isolation of nucleon properties.[22]

Recent computations of the isovector axial charge with a complete stated error budget include: $g_A = 1.195(20)(33)$ [100], where the first error is due to extrapolating in lattice spacing, lattice volume and light quark masses, and the second error is statistical and other systematics; and $g_A = 1.278(21)(26)$ [98], where the first error is statistical and fitting systematics, and the second error is due to model selection in the chiral and continuum extrapolation. Other recent preliminary results and discussions may be found in Refs. [21, 22, 101–106]. We remark that QED radiative corrections are below the current lattice QCD sensitivity, and the details of the g_A definition in the presence of radiative corrections are thus not yet relevant for this comparison. Note also that the isovector quark current is scale independent in the usual $\overline{\text{MS}}$ scheme used to present lattice results.

Lattice QCD is approaching the few percent level for g_A. A complete calculation of r_A^2 that would rival the precision of neutrino-nucleon scattering and muon capture is not yet available from lattice QCD. However, illustrative values have been obtained, typically using simplified functional forms for the q^2 behavior, unphysically large light quark masses, and/or neglect of strange and charm quarks. A dipole form factor ansatz fit to two-flavor lattice QCD extractions of $F_A(q^2)$ [22] found a result, $r_A^2 = 0.266(17)(7)\,\text{fm}^2$, where the first error is statistical and the second is systematic due to excited states; this result lies closer to the "large m_A" MiniBooNE dipole result [20] than to the "small m_A" historical dipole average [17, 107]. A z expansion fit to $F_A(q^2)$ obtained using three-flavor QCD with physical strange quark mass, and heavier-than-physical up and down quark masses (corresponding to pion mass 317 MeV) [21], yielded $r_A^2 = 0.213(6)(13)(3)(0)\,\text{fm}^2$, where the uncertainties are from statistics, excited states, fitting and renormalization. A first order z expansion fit to $F_A(q^2)$ using two-flavor QCD, extrapolated to physical pion mass [23] yielded $r_A^2 = 0.360(36)^{+80}_{-88}\,\text{fm}^2$, where the first error is statistical and the second error is systematic. Finally, a z expansion fit to four-flavor lattice QCD data using a range of lattice parameters [24] yielded $r_A^2 = 0.24(6)\,\text{fm}^2$. Some of these r_A^2 values are well below the historical dipole value and even disagree somewhat with our conservative average of $r_A^2(\text{avg.}) = 0.45(16)\ \text{fm}^2$ in Eq. (36). This situation suggests that either remaining lattice corrections, such as extrapolations to physical pion mass, will involve large corrections that significantly shift the lattice determinations, or perhaps more exciting that a disagreement may persist as further lattice progress is made, leading to a new paradigm in our understanding of r_A^2. However, at this point, further work is needed to obtain precise lattice results with more complete error budgets.

5.2.2 Pion electroproduction

Fits to pion electroproduction data have historically contributed to the determination of the axial radius, with a small quoted uncertainty that can be traced to the assumed dipole form factor constraint. The statistical power of available data would be comparable to the neutrino-deuteron scattering determination, but relies on extrapolations beyond the regime of low energies where chiral corrections are controlled. The axial form factor appears in a low energy theorem for the S-wave electric dipole amplitude of threshold charged pion electroproduction ($e^- p \to e^- n \pi^+$) [108, 109],

$$E_{0+}^{(-)}\big|_{m_\pi=0} = \sqrt{1 - \frac{q^2}{4m_N^2}}\,\frac{e g_A}{8\pi f_\pi}\left[F_A(q^2) + \frac{q^2}{4m_N^2 - 2q^2}F_M(q^2)\right]. \tag{41}$$

This low energy theorem is strictly valid in the chiral limit ($m_\pi = 0$) for threshold production (invariant mass $W = m_N + m_\pi$ in final state hadronic system). The chiral and threshold limits do not commute, but corrections to the low energy theorem may be calculated within χPT [110]. Two complications enter.

[22] For recent examples and further references, see Refs. [95–99].

First, experimental measurement is difficult, involving the detection of either a recoiling neutron or a low energy pion. Most of the statistical power of available data involves energies and momentum transfers outside of the regime where a chiral expansion is reliable. The data have been interpreted in terms of a phenomenological framework, whose associated systematic uncertainty is difficult to assess. Second, taking at face value the phenomenological extraction of $F_A(q^2)$ at certain kinematic points from the experimental data, the interpretation as a measurement of the radius has assumed a dipole shape that strongly influences the result.

Using the extracted form factor values at particular kinematic points from Refs. [111–115], but replacing dipole with z expansion, Ref. [18] obtained $r_A^2 = 0.55(17)\,\mathrm{fm}^2$, compared to the dipole analysis of Ref. [107] which gave $r_A^2 = 0.467(18)\,\mathrm{fm}^2$. The datasets were selected to coincide with those that appear in the compilation [107] in order to make a direct comparison with their dipole fit (cf. Figure 1 of that reference). These datasets explicitly list inferred values of $F_A(q^2)$ (see also [116–120]). Reference [120] provides a value $r_A^2 = 0.449(28)\,\mathrm{fm}^2$ based on data at $W = 1125\,\mathrm{MeV}$ and $Q^2 = 0.117$, 0.195 and $0.273\,\mathrm{GeV}^2$, and a phenomenological Lagrangian analysis.[23] Reference [121] presents data at $W = 1094\,\mathrm{MeV}$ and $Q^2 = 0.078\,\mathrm{GeV}^2$. Regardless of the precise choice of dataset, the error is significantly larger when the strict dipole assumption is relaxed, even when systematics associated with extrapolations outside of the chiral Lagrangian framework are neglected. Further effort is needed before pion electroproduction provides a robust answer for r_A^2.

5.2.3 Lepton scattering

Since the most direct constraints on $F_A(q^2)$ come from neutrino scattering data, it is natural to ask whether improved measurements are feasible. The world dataset for neutrino deuteron scattering consists of a few thousand quasielastic events from bubble chamber data of the 1970s and 1980s. Systematic uncertainties from hand-scanning of photographs and from nuclear modeling are comparable to statistical errors, contributing to the total quoted uncertainty on r_A^2 of $0.22\,\mathrm{fm}^2$ in Ref. [19]. Note that the flux is determined self consistently from the quasielastic events, so that flux errors associated with neutrino production are not relevant. Although nuclear corrections for deuteron targets are relatively small compared to heavier nuclei, errors are difficult to quantify at the desired few percent level, for accelerator neutrino beams of GeV energies. Antineutrino data on hydrogen would eliminate even these relatively small corrections. Existing antineutrino quasielastic data is very sparse, owing to the combined penalties of smaller production cross section for creating antineutrino versus neutrino beams, and smaller scattering cross section for antineutrinos versus neutrinos. Thus most data was taken in neutrino mode versus antineutrino mode. Reference [122] reported 13 ± 6 events. References [123, 124] reported results for antineutrino-proton scattering inferred from data taken on nuclear (carbon) targets. Currently available analysis techniques with an active target detector should reduce or eliminate scanning and efficiency systematic corrections. Modern neutrino beams have much higher flux compared to the beams used for the existing datasets which would enable either a much smaller detector or a much larger dataset over a given timescale. Technical, cost and safety considerations must be addressed in order to make such a new measurement feasible.

The capture process $\mu^- p \to \nu_\mu n$ in muonic hydrogen, and the time reversed process $\nu_\mu n \to \mu^- p$ measured in neutrino scattering, both probe the charged-current component of the isovector axial vector nucleon matrix element. By isospin symmetry, this isovector matrix element can also be accessed via the neutral component. Parity violating electron-nucleon elastic scattering [125, 126], induced by weak Z^0 exchange, is a probe of this matrix element, but simultaneously involves also isoscalar and strange quark contributions that must be independently constrained. Available data do not have discriminating power to reliably extract axial radius or form factor shape information. For example, the G0 experiment [126] analyzed electron-proton and electron-deuteron scattering data to perform a simultaneous fit

[23] This result is obtained from the dipole axial mass $m_A = 1.077(39)$, after applying the chiral correction $\delta r_A^2 = 0.046\,\mathrm{fm}^2$ [107].

of the isovector axial form factor, and the strange vector form factors, taking the remaining form factors from other sources. An amplitude was measured for $F_A(q^2)$ at $Q^2 = -q^2 = 0.22$ and 0.63 GeV^2, but with insufficient precision to extract shape information. The process $e^+d \to \bar{\nu}_e pp$ is another possibility to access the charged current nucleon interaction, $e^+n \to \bar{\nu}_e p$ using electron (positron) beams. No measurements of this process currently exist.

5.2.4 Summary of complementary constraints

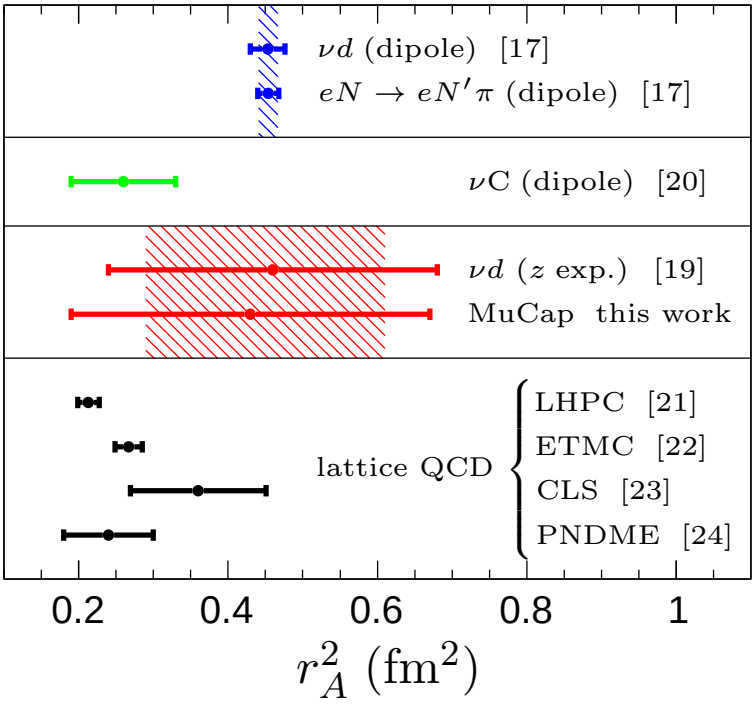

Figure 7: (color online) Axial radius determined by different processes. Data points are as in Table 1. The hashed red region represents the average of the z expansion νd and MuCap results [cf. Eq. (36)]. The hatched blue band represents the average of the dipole νd and dipole $eN \to eN'\pi$ results from Ref. [17].

A range of processes and techniques have potential to help constrain the nucleon axial radius. Some of these, such as pion electroproduction and parity violating electron-proton scattering, access the form factor and radius indirectly and suffer significant model-dependent corrections that need to be further addressed to achieve $\sim 10\%$ accuracy on r_A^2. Lattice QCD and elementary target neutrino scattering are potentially pristine theoretical or experimental approaches. However, lattice QCD has not yet achieved the requisite accuracy, and hydrogen or deuterium active target neutrino experiments are fraught with surmountable but difficult technical and safety issues. Figure 7 displays the range of values for r_A^2 as tabulated in Table 1, along with the MuCap determination presented in this paper. The future is sure to witness an interesting complementarity between different approaches to axial nucleon structure, with a wide range of constraints and applications.

6 Summary and outlook

In this paper we considered the status and prospects of constraints on the isovector axial nucleon form factor, $F_A(q^2)$, which describes a range of lepton-nucleon reactions. We focused in particular on its prominent role in neutrino-nucleus scattering cross sections underlying neutrino oscillation experiments at accelerator energies. A precise knowledge of these cross sections, for momentum transfers $|q^2| \lesssim$ few GeV^2, is required for the next generation of precision studies of neutrino properties in long baseline oscillation experiments. Fully utilizing the oscillation data will require better knowledge of the structure of $F_A(q^2)$, in concert with data-driven improvements in heavy nuclear target modeling.

For many processes, the first two terms in the q^2 expansion of $F_A(q^2)$ can be shown to dominate. These terms are parameterized by $g_A \equiv F_A(0)$, and r_A^2, which is proportional to the slope of $F_A(q^2)$ at $q^2 \to 0$. The axial nucleon coupling, g_A, is precisely determined from neutron beta decay; we use g_A=1.2749(9) in this work. The nucleon axial radius squared, r_A^2, was considered well-determined and uncontroversial for a long time, with $r_A^2(\text{dipole}) = 0.454(13)\,\text{fm}^2$, derived from a dipole fit to neutrino scattering and pion electro-production data. A recent analysis, however, eliminated the dipole shape constraint for $F_A(q^2)$, as not justifiable from first principles. Using instead the z expansion as a model independent formalism to enforce properties inherited from the underlying QCD structure, a value $r_A^2(z\text{ exp.}, \nu)$=0.46(22) fm^2 was derived [106] from a fit to the νd scattering data. The more conservative, but better justified error is an order of magnitude larger than that from the dipole fit, with nearly 50% uncertainty. In this work we assessed some ramifications of this new development, and in particular reviewed and suggested opportunities to reduce the uncertainty in r_A^2.

We started from the vantage point of muon capture, in particular muon capture in the theoretically pristine atom of muonic hydrogen, μH. Muon capture is a charged-current reaction with a small momentum transfer, $q_0^2 \approx -0.9\,m_\mu^2$, so that $F_A(q_0^2)$ is only $\sim 2\%$ smaller than $F_A(0)$. In the past, the uncertainty introduced by the error in r_A^2(dipole) was considered negligible, and capture in μH was used to determine the nucleon pseudoscalar coupling $\bar{g}_P$. The recent 1% MuCap measurement of the spin singlet muonic hydrogen capture rate, $\Lambda_{\text{singlet}}^{\text{MuCap}} = 715.6(7.4)\,\text{s}^{-1}$, determined $\bar{g}_P^{\text{MuCap}} = 8.06(55)$, using theory and form factors available at the time. The agreement of this result with the precise prediction of χPTis considered an important test of the chiral structure of QCD. Given the dramatically increased uncertainty in r_A^2, we addressed the following questions, answering both in the affirmative: Does the comparison of $\bar{g}_P$ between experiment and theory still provide a robust test of χPT? And, in a reversal of strategy, can muon capture be used to determine a competitive value of r_A^2?

High precision is required both in theory and experiment to utilize the small effect of r_A^2 on muon capture. In this paper, we have reduced the uncertainty in the electroweak radiative corrections to muon capture to the 0.14% level and extracted an updated value, $\bar{g}_P^{\text{MuCap}} = 8.19(84)$, from the MuCap experiment. Agreement with the updated theoretical prediction from χPT, $\bar{g}_P^{\text{theory}} = 8.25(25)$, remains excellent. It confirms expectations at a sensitivity level of $\pm 8\%$, weakened only slightly (from $\pm 6\%$) by the larger uncertainty in $r_A^2(z\text{ exp.}, \nu)$ compared to r_A^2(dipole). The MuCap result was also used to provide a self-consistent test of the pion-nucleon coupling and to obtain a roughly $\pm 1\%$ muon-based value of g_A, which was found to be in agreement with the electron-based value traditionally extracted fron neutron decay (thereby, testing electron-muon universality). Of course, all such tests would be improved by a better independent determination of r_A^2 and the factor of 3 improvement in a next generation muon capture experiment advocated here.

As a novel application of the muonic Hydrogen capture rate, we explored its use as an alternative method for determining the nucleon axial radius squared. Using the rather precise theoretical expression for $\bar{g}_P^{\text{theory}}$ from χPT, along with updated radiative corrections and form factors as input, we found $r_A^2(\mu\text{H}) = 0.43(24)\text{fm}^2$ from the MuCap singlet capture rate measurement. Combining that finding with the z expansion neutrino-nucleon scattering result led to a weighted average $r_A^2(\text{ave.}) = 0.45(16)\text{fm}^2$. We also examined the possibility of improving the MuCap experiment by roughly a factor of 3 and thereby determining r_A^2 to about $\pm 20\%$. As demonstrated, that level of accuracy would be sufficient to reduce

the r_A^2 induced uncertainties in neutrino-nucleon scattering to a subdominant level. Moreover, it would start to become a standard for comparison with other methods of r_A^2 determination, several of which were discussed. For such comparisons, lattice gauge theory calculations appear to hold the most promise. Although that Monte Carlo approach to QCD is still not fully mature as applied to r_A^2, it promises a first principles strong coupling method that in time should reach high precision. Some early current efforts seem to suggest a significantly smaller value of r_A^2 compared to historical dipole averages, but it is still too early to scrutinize or average the lattice results in a meaningful way. Future confrontation between experiment and lattice QCD will be interesting to watch and could provide surprises.

The nucleon axial radius has reached an exciting new stage. Until recently, it was thought to be well determined by dipole form factor fits to neutrino-nucleon scattering and electroproduction measurements. However, driven especially by the need for better neutrino cross section predictions, that common lore has been replaced by more conservative healthy skepticism. The axial vector form factor is now being approached from many directions, with the potential to challenge conventional dogma as it enters a new precision era.

Acknowledgments

We thank M. Hoferichter for helpful discussion of the pion-nucleon coupling. R. J. H. thanks TRIUMF for hospitality where a part of this work was performed. Research of R. J. H. was supported by a NIST Precision Measurement Grant. Research at Perimeter Institute is supported by the Government of Canada through the Department of Innovation, Science and Economic Development and by the Province of Ontario through the Ministry of Research and Innovation. Fermilab is operated by Fermi Research Alliance, LLC under Contract No. DE-AC02-07CH11359 with the United States Department of Energy. The work of P. K. was supported by the U.S. Department of Energy Office of Science, Office of Nuclear Physics under Award Number DE-FG02-97ER41020. The work of W. J. M. was supported by the U.S. Department of Energy under grant DE-SC0012704. The work of A. S. was supported in part by the National Science Foundation under Grant PHY-1620039.

References

[1] R. Pohl *et al.*, Nature **466**, 213 (2010).

[2] A. Antognini *et al.*, Science **339**, 417 (2013).

[3] P. J. Mohr, B. N. Taylor, and D. B. Newell, Rev. Mod. Phys. **84**, 1527 (2012), arXiv:1203.5425 [physics.atom-ph].

[4] R. Pohl, R. Gilman, G. A. Miller, and K. Pachucki, Ann. Rev. Nucl. Part. Sci. **63**, 175 (2013), arXiv:1301.0905 [physics.atom-ph].

[5] C. E. Carlson, Prog. Part. Nucl. Phys. **82**, 59 (2015), arXiv:1502.05314 [hep-ph].

[6] R. J. Hill, *Proceedings, 12th Conference on Quark Confinement and the Hadron Spectrum (Confinement XII): Thessaloniki, Greece*, EPJ Web Conf. **137**, 01023 (2017), arXiv:1702.01189 [hep-ph].

[7] P. Kammel and K. Kubodera, Ann. Rev. Nucl. Part. Sci. **60**, 327 (2010).

[8] D. H. Wright *et al.*, Phys. Rev. **C57**, 373 (1998).

[9] S. L. Adler and Y. Dothan, Phys. Rev. **151**, 1267 (1966).

[10] L. Wolfenstein, *High Energy Physics and Nuclear Structure* (Plenum, New York, 1970) p. 661.

[11] V. Bernard, N. Kaiser, and U. G. Meissner, Phys. Rev. **D50**, 6899 (1994), arXiv:hep-ph/9403351 [hep-ph].

[12] V. Bernard, T. R. Hemmert, and U.-G. Meissner, Nucl. Phys. **A686**, 290 (2001), arXiv:nucl-th/0001052 [nucl-th].

[13] N. Kaiser, Phys. Rev. **C67**, 027002 (2003), arXiv:nucl-th/0301034 [nucl-th].

[14] V. Andreev *et al.*, Phys. Rev. Lett. **110**, 012504 (2013), arXiv:1210.6545 [nucl-ex].

[15] V. A. Andreev *et al.*, Phys. Rev. **C91**, 055502 (2015), arXiv:1502.00913 [nucl-ex].

[16] A. Czarnecki, W. J. Marciano, and A. Sirlin, Phys. Rev. Lett. **99**, 032003 (2007), arXiv:0704.3968 [hep-ph].

[17] A. Bodek, S. Avvakumov, R. Bradford, and H. S. Budd, Eur. Phys. J. **C53**, 349 (2008), arXiv:0708.1946 [hep-ex].

[18] B. Bhattacharya, R. J. Hill, and G. Paz, Phys. Rev. **D84**, 073006 (2011), arXiv:1108.0423 [hep-ph].

[19] A. S. Meyer, M. Betancourt, R. Gran, and R. J. Hill, Phys. Rev. **D93**, 113015 (2016), arXiv:1603.03048 [hep-ph].

[20] A. A. Aguilar-Arevalo *et al.*, Phys. Rev. **D81**, 092005 (2010), arXiv:1002.2680 [hep-ex].

[21] J. Green, N. Hasan, S. Meinel, M. Engelhardt, S. Krieg, J. Laeuchli, J. Negele, K. Orginos, A. Pochinsky, and S. Syritsyn, Phys. Rev. **D95**, 114502 (2017), arXiv:1703.06703 [hep-lat].

[22] C. Alexandrou, M. Constantinou, K. Hadjiyiannakou, K. Jansen, C. Kallidonis, G. Koutsou, and A. Vaquero Aviles-Casco, (2017), arXiv:1705.03399 [hep-lat].

[23] S. Capitani, M. Della Morte, D. Djukanovic, G. M. von Hippel, J. Hua, B. Jäger, P. M. Junnarkar, H. B. Meyer, T. D. Rae, and H. Wittig, (2017), arXiv:1705.06186 [hep-lat].

[24] R. Gupta, Y.-C. Jang, H.-W. Lin, B. Yoon, and T. Bhattacharya, (2017), arXiv:1705.06834 [hep-lat].

[25] R. J. Hill and G. P. Lepage, Phys. Rev. **D62**, 111301 (2000), arXiv:hep-ph/0003277 [hep-ph].

[26] G. P. Lepage, in *Nuclear physics. Proceedings, 8th Jorge Andre Swieca Summer School, Sao Jose dos Campos, Campos do Jordao, Brazil, January 26-February 7, 1997* (1997) pp. 135–180, arXiv:nucl-th/9706029 [nucl-th].

[27] M. I. Eides, H. Grotch, and V. A. Shelyuto, Phys. Rept. **342**, 63 (2001), arXiv:hep-ph/0002158 [hep-ph].

[28] D. Eiras and J. Soto, Phys. Lett. **B491**, 101 (2000), arXiv:hep-ph/0005066 [hep-ph].

[29] V. A. Andreev *et al.*, Phys. Rev. Lett. **99**, 032002 (2007), arXiv:0704.2072 [nucl-ex].

[30] H. Shiomi, Nucl. Phys. **A603**, 281 (1996), arXiv:hep-ph/9601329 [hep-ph].

[31] J. Govaerts and J.-L. Lucio-Martinez, Nucl. Phys. **A678**, 110 (2000), arXiv:nucl-th/0004056 [nucl-th].

[32] K. Minamisono *et al.*, Phys. Rev. **C65**, 015501 (2002).

[33] B. R. Holstein, J. Phys. **G41**, 114001 (2014).

[34] A. Santisteban and R. Pascual, Nucl. Phys. **A260**, 392 (1976).

[35] U. Raha, F. Myhrer, and K. Kubodera, Phys. Rev. **C87**, 055501 (2013), arXiv:1303.6247 [nucl-th].

[36] S. Pastore, F. Myhrer, and K. Kubodera, Phys. Rev. **C88**, 058501 (2013), arXiv:1309.4425 [nucl-th].

[37] S. Pastore, F. Myhrer, and K. Kubodera, Int. J. Mod. Phys. **E23**, 1430010 (2014), arXiv:1405.1358 [nucl-th].

[38] A. Sirlin, Rev. Mod. Phys. **50**, 573 (1978), [Erratum: Rev. Mod. Phys.50,905(1978)].

[39] V. Tishchenko *et al.*, Phys. Rev. **D87**, 052003 (2013), arXiv:1211.0960 [hep-ex].

[40] J. C. Hardy and I. S. Towner, Phys. Rev. **C91**, 025501 (2015), arXiv:1411.5987 [nucl-ex].

[41] W. J. Marciano and A. Sirlin, Phys. Rev. Lett. **96**, 032002 (2006), arXiv:hep-ph/0510099 [hep-ph].

[42] A. Czarnecki, W. J. Marciano, and A. Sirlin, Phys. Rev. **D70**, 093006 (2004), arXiv:hep-ph/0406324 [hep-ph].

[43] C. Patrignani *et al.*, Chin. Phys. **C40**, 100001 (2016).

[44] R. E. Behrends and A. Sirlin, Phys. Rev. Lett. **4**, 186 (1960).

[45] M. Terentev, Zh. Eksperim. i Teor. Fiz. **44**, 1320 (1963), [Sov.Phys. JETP **17**, 890 (1963)].

[46] M. Ademollo and R. Gatto, Phys. Rev. Lett. **13**, 264 (1964).

[47] A. Sirlin, Phys. Rev. **164**, 1767 (1967).

[48] J. L. Friar, Annals Phys. **122**, 151 (1979).

[49] V. Baru, C. Hanhart, M. Hoferichter, B. Kubis, A. Nogga, and D. R. Phillips, Phys. Lett. **B694**, 473 (2011), arXiv:1003.4444 [nucl-th].

[50] V. Baru, C. Hanhart, M. Hoferichter, B. Kubis, A. Nogga, and D. R. Phillips, Nucl. Phys. **A872**, 69 (2011), arXiv:1107.5509 [nucl-th].

[51] P. J. Mohr, D. B. Newell, and B. N. Taylor, Rev. Mod. Phys. **88**, 035009 (2016), arXiv:1507.07956 [physics.atom-ph].

[52] Z. Epstein, G. Paz, and J. Roy, Phys. Rev. **D90**, 074027 (2014), arXiv:1407.5683 [hep-ph].

[53] G. Lee, J. R. Arrington, and R. J. Hill, Phys. Rev. **D92**, 013013 (2015), arXiv:1505.01489 [hep-ph].

[54] J. C. Bernauer *et al.*, Phys. Rev. **C90**, 015206 (2014), arXiv:1307.6227 [nucl-ex].

[55] R. J. Hill and G. Paz, Phys. Rev. **D82**, 113005 (2010), arXiv:1008.4619 [hep-ph].

[56] M. A. Belushkin, H. W. Hammer, and U. G. Meissner, Phys. Rev. **C75**, 035202 (2007), arXiv:hep-ph/0608337 [hep-ph].

[57] D. H. Wilkinson, Nucl. Phys. **A377**, 474 (1982).

[58] F. E. Wietfeldt and G. L. Greene, Reviews of Modern Physics **83**, 1173 (2011).

[59] W. A. Mann *et al.*, Phys. Rev. Lett. **31**, 844 (1973).

[60] S. J. Barish *et al.*, Phys. Rev. **D16**, 3103 (1977).

[61] K. L. Miller *et al.*, Phys. Rev. **D26**, 537 (1982).

[62] N. J. Baker, A. M. Cnops, P. L. Connolly, S. A. Kahn, H. G. Kirk, M. J. Murtagh, R. B. Palmer, N. P. Samios, and M. Tanaka, Phys. Rev. **D23**, 2499 (1981).

[63] T. Kitagaki *et al.*, Phys. Rev. **D28**, 436 (1983).

[64] T. Kitagaki *et al.*, Phys. Rev. **D42**, 1331 (1990).

[65] J. J. de Swart, M. C. M. Rentmeester, and R. G. E. Timmermans, *Meson nucleon physics and the structure of the nucleon. Proceedings, 7th International Symposium, MENU'97, Vancouver, Canada, July 28-August 1, 1997*, PiN Newslett. **13**, 96 (1997), arXiv:nucl-th/9802084 [nucl-th].

[66] R. A. Arndt, W. J. Briscoe, I. I. Strakovsky, R. L. Workman, and M. M. Pavan, Phys. Rev. **C69**, 035213 (2004), arXiv:nucl-th/0311089 [nucl-th].

[67] R. A. Arndt, W. J. Briscoe, I. I. Strakovsky, and R. L. Workman, Phys. Rev. **C74**, 045205 (2006), arXiv:nucl-th/0605082 [nucl-th].

[68] T. Gorringe and H. W. Fearing, Rev. Mod. Phys. **76**, 31 (2004), arXiv:nucl-th/0206039 [nucl-th].

[69] A. Czarnecki, W. J. Marciano, and K. Melnikov, *Physics at the first muon collider and at the front end of a muon collider. Proceedings, Workshop, Batavia, USA, November 6-9, 1997*, AIP Conf. Proc. **435**, 409 (1998), arXiv:hep-ph/9801218 [hep-ph].

[70] D. D. Bakalov, M. P. Faifman, L. I. Ponomarev, and S. I. Vinitsky, Nucl. Phys. **A384**, 302 (1982).

[71] P. Ackerbauer *et al.*, Phys. Lett. **B417**, 224 (1998), arXiv:hep-ph/9708487 [hep-ph].

[72] L. Marcucci, A. Kievsky, S. Rosati, R. Schiavilla, and M. Viviani, Phys. Rev. Lett. **108**, 052502 (2012), arXiv:1109.5563 [nucl-th].

[73] V. A. Andreev *et al.*, (2010), arXiv:1004.1754 [nucl-ex].

[74] J.-W. Chen, K. M. Heeger, and R. G. H. Robertson, Phys. Rev. **C67**, 025801 (2003), arXiv:nucl-th/0210073 [nucl-th].

[75] G. Bardin, J. Duclos, A. Magnon, J. Martino, A. Richter, E. Zavattini, A. Bertin, M. Piccinini, A. Vitale, and D. F. Measday, Nucl. Phys. **A352**, 365 (1981).

[76] J. Egger *et al.*, Eur. Phys. J. **A50**, 163 (2014), arXiv:1405.2853 [physics.ins-det].

[77] V. A. Ganzha *et al.*, Nucl. Instrum. Meth. **A578**, 485 (2007), arXiv:0705.1473 [nucl-ex].

[78] I. Alekseev *et al.*, Rev. Sci. Instrum. **86**, 125102 (2015).

[79] M. Döbeli, M. Ruff, M. Suter, H.-A. Synal, E. von Wartburg and L. Wacker, Nucl. Instrum. Meth. **B266**, 1820 (2008).

[80] M. J. Barnes and G. D. Wait, IEEE Trans. Plasma Sci. **32**, 1932 (2004).

[81] K. Hikasa *et al.*, Phys. Rev. **D45**, S1 (1992), [Erratum: Phys. Rev.D46,5210(1992)].

[82] R. A. Ryan *et al.*, JINST **9**, P07029 (2014), arXiv:1404.3251 [physics.ins-det].

[83] H. Abele, Prog. Part. Nucl. Phys. **60**, 1 (2008).

[84] D. Dubbers and M. G. Schmidt, Rev. Mod. Phys. **83**, 1111 (2011), arXiv:1105.3694 [hep-ph].

[85] R. W. Pattie *et al.*, (2017), arXiv:1707.01817 [nucl-ex].

[86] I. V. Anikin, V. M. Braun, and N. Offen, Phys. Rev. **D94**, 034011 (2016), arXiv:1607.01504 [hep-ph].

[87] C. Adams *et al.*, (2013), arXiv:1307.7335 [hep-ex].

[88] R. Acciarri *et al.*, (2015), arXiv:1512.06148 [physics.ins-det].

[89] M. V. Diwan, V. Galymov, X. Qian, and A. Rubbia, Ann. Rev. Nucl. Part. Sci. **66**, 47 (2016), arXiv:1608.06237 [hep-ex].

[90] U. Mosel, Ann. Rev. Nucl. Part. Sci. **66**, 171 (2016), arXiv:1602.00696 [nucl-th].

[91] T. Katori and M. Martini, (2016), arXiv:1611.07770 [hep-ph].

[92] L. Alvarez-Ruso *et al.*, (2017), arXiv:1706.03621 [hep-ph].

[93] S. Aoki *et al.*, Eur. Phys. J. **C77**, 112 (2017), arXiv:1607.00299 [hep-lat].

[94] G. P. Lepage, in *From actions to answers. Proceedings, Theoretical Advanced Study Institute in Elementary Particle Physics, Boulder, USA, June 5-30, 1989*, edited by T. A. DeGrand and D. Toussaint (1990) pp. 97–120.

[95] B. C. Tiburzi, M. L. Wagman, F. Winter, E. Chang, Z. Davoudi, W. Detmold, K. Orginos, M. J. Savage, and P. E. Shanahan, (2017), arXiv:1702.02929 [hep-lat].

[96] M. J. Savage, P. E. Shanahan, B. C. Tiburzi, M. L. Wagman, F. Winter, S. R. Beane, E. Chang, Z. Davoudi, W. Detmold, and K. Orginos, Phys. Rev. Lett. **119**, 062002 (2017), arXiv:1610.04545 [hep-lat].

[97] C. Bouchard, C. C. Chang, T. Kurth, K. Orginos, and A. Walker-Loud, Phys. Rev. **D96**, 014504 (2017), arXiv:1612.06963 [hep-lat].

[98] E. Berkowitz *et al.*, (2017), arXiv:1704.01114 [hep-lat].

[99] C. Alexandrou, *Proceedings, 12th Conference on Quark Confinement and the Hadron Spectrum (Confinement XII): Thessaloniki, Greece*, EPJ Web Conf. **137**, 01004 (2017), arXiv:1612.04644 [hep-lat].

[100] T. Bhattacharya, V. Cirigliano, S. Cohen, R. Gupta, H.-W. Lin, and B. Yoon, Phys. Rev. **D94**, 054508 (2016), arXiv:1606.07049 [hep-lat].

[101] M. Abramczyk, M. Lin, A. Lytle, and S. Ohta, *Proceedings, 34th International Symposium on Lattice Field Theory (Lattice 2016): Southampton, UK, July 24-30, 2016*, PoS **LATTICE2016**, 150 (2016), arXiv:1610.09773 [hep-lat].

[102] T. Yamazaki, *Proceedings, 33rd International Symposium on Lattice Field Theory (Lattice 2015): Kobe, Japan, July 14-18, 2015*, PoS **LATTICE2015**, 081 (2016), arXiv:1511.09179 [hep-lat].

[103] J. Liang, Y.-B. Yang, K.-F. Liu, A. Alexandru, T. Draper, and R. S. Sufian, (2016), arXiv:1612.04388 [hep-lat].

[104] A. Abdel-Rehim *et al.*, Phys. Rev. **D92**, 114513 (2015), [Erratum: Phys. Rev.D93,no.3,039904(2016)], arXiv:1507.04936 [hep-lat].

[105] D. Djukanovic, T. Harris, G. von Hippel, P. Junnarkar, H. B. Meyer, and H. Wittig, *Proceedings, 34th International Symposium on Lattice Field Theory (Lattice 2016): Southampton, UK, July 24-30, 2016*, PoS **LATTICE2016**, 167 (2017), arXiv:1611.07918 [hep-lat].

[106] A. S. Meyer, R. J. Hill, A. S. Kronfeld, R. Li, and J. N. Simone, *Proceedings, 34th International Symposium on Lattice Field Theory (Lattice 2016): Southampton, UK, July 24-30, 2016*, PoS **LATTICE2016**, 179 (2016), arXiv:1610.04593 [hep-lat].

[107] V. Bernard, L. Elouadrhiri, and U.-G. Meissner, J. Phys. **G28**, R1 (2002), arXiv:hep-ph/0107088 [hep-ph].

[108] Y. Nambu and D. Lurie, Phys. Rev. **125**, 1429 (1962).

[109] Y. Nambu and E. Shrauner, Phys. Rev. **128**, 862 (1962).

[110] V. Bernard, N. Kaiser, and U. G. Meissner, Phys. Rev. Lett. **69**, 1877 (1992).

[111] E. Amaldi, M. Benevantano, B. Borgia, F. De Notaristefani, A. Frondaroli, P. Pistilli, I. Sestili, and M. Severi, Phys. Lett. **41B**, 216 (1972).

[112] P. Brauel *et al.*, Phys. Lett. **45B**, 389 (1973).

[113] A. Del Guerra, A. Giazotto, M. A. Giorgi, A. Stefanini, D. R. Botterill, D. W. Braben, D. Clarke, and P. R. Norton, Nucl. Phys. **B99**, 253 (1975).

[114] A. Del Guerra, A. Giazotto, M. A. Giorgi, A. Stefanini, D. R. Botterill, H. E. Montgomery, P. R. Norton, and G. Matone, Nucl. Phys. **B107**, 65 (1976).

[115] A. S. Esaulov, A. M. Pilipenko, and Yu. I. Titov, Nucl. Phys. **B136**, 511 (1978).

[116] E. Amaldi, B. Borgia, P. Pistilli, M. Balla, G. V. Di Giorgio, A. Giazotto, S. Serbassi, and G. Stoppini, Nuovo Cim. **A65**, 377 (1970).

[117] E. D. Bloom, R. L. Cottrell, H. C. DeStaebler, C. L. Jordan, H. Piel, C. Y. Prescott, R. Siemann, S. Stein, and R. E. Taylor, Phys. Rev. Lett. **30**, 1186 (1973).

[118] P. Joos *et al.*, Phys. Lett. **B62**, 230 (1976).

[119] S. Choi *et al.*, Phys. Rev. Lett. **71**, 3927 (1993).

[120] A. Liesenfeld *et al.*, Phys. Lett. **B468**, 20 (1999), arXiv:nucl-ex/9911003 [nucl-ex].

[121] I. Friščić *et al.*, Phys. Lett. **B766**, 301 (2017), arXiv:1606.00970 [nucl-ex].

[122] G. Fanourakis, L. K. Resvanis, G. Grammatikakis, P. Tsilimigras, A. Vayaki, U. Camerini, W. F. Fry, R. J. Loveless, J. H. Mapp, and D. D. Reeder, Phys. Rev. **D21**, 562 (1980).

[123] L. A. Ahrens *et al.*, Phys. Rev. **D35**, 785 (1987).

[124] L. A. Ahrens *et al.*, Phys. Lett. **B202**, 284 (1988).

[125] E. J. Beise, M. L. Pitt, and D. T. Spayde, Prog. Part. Nucl. Phys. **54**, 289 (2005), arXiv:nucl-ex/0412054 [nucl-ex].

[126] D. Androic *et al.*, Phys. Rev. Lett. **104**, 012001 (2010), arXiv:0909.5107 [nucl-ex].